International Journal of
*Molecular Sciences*

MDPI

*Article*

# Dual Anticancer and Antibacterial Applications of Active Particle Aggregates Containing Metal Phthalocyanines in Dark

**Laila Jaragh-Alhdadad [1,2,*], Moayyad Alsawah [1] and Rasheed Ahmad [2]**

[1] Department of Chemistry, College of Science, Kuwait University, Sabah Al Salem University City, Shadadiya, Kuwait City 13060, Kuwait
[2] Immunology & Microbiology Department, Dasman Diabetic Institute, Dasman, Kuwait City 15462, Kuwait
* Correspondence: laila.alhadad@ku.edu.kw

**Abstract**

Cancer is still a significant worldwide health concern, and the side effects of traditional chemotherapy emphasize the need for safer and more potent treatment methods. The structural diversity and specific biological action of bioorganic molecules make them essential components of many anticancer medications. Therefore, the anticancer and antibacterial activity of metal phthalocyanine agents were designed, synthesized, thoroughly characterized, and assessed in this study. These agents were loaded in both natural and artificial nanoparticles, such as chitosan (Chi), polyethylene glycol (PEG), and low-density lipoprotein (LDL), to improve therapeutic efficacy. Morphological and physicochemical properties were assessed using scanning electron microscopy (SEM), dynamic light scattering (DLS), energy-dispersive X-ray (EDX), and thermal gravimetric analysis (TGA). Complexes formed were increased in particle size and improved biological efficacy. Both free and metal phthalocyanine complexes were tested against breast (MDA-MB-453) and liver cancer (HEPG2) cell lines and *Escherichia coli* (*E. coli)* bacteria, with metal phthalocyanine complex formulations showing superior activity. Notably, gallium phthalocyanine (II) showed the strongest anticancer and antibacterial properties, indicating its potential as a promising future treatment option without light activation.

**Keywords:** metal phthalocyanine; particle aggregates; drug delivery; chitosan; PEG; LDL; anticancer assessment; antibacterial activity

## 1. Introduction

Cancer and bacterial infections remain major health challenges due to their high mortality rates, necessitating extensive scientific investigation [1–3]. In recent years, a variety of organic compounds, including phthalocyanine [4], pyrazole [1], hydrazine [5,6], thiazole [7,8], triazole [3], and pyrimidine derivatives [9,10], have been investigated for their potential as anticancer and antibacterial agents [3,11]. These compounds exhibit diverse biological activities, including antibacterial, anticancer, antimalarial, anti-Alzheimer's, and antiviral properties [12–14]. Current research is directed toward optimizing their molecular structures, solubility, and targeting capabilities to improve therapeutic efficacy and selectivity while reducing undesirable side effects [15,16].

Phthalocyanine is a synthetic macrocyclic molecule that shares structural similarities with the porphyrins found in heme and chlorophyll [4]. It has a central cavity that allows $\pi$–$\pi$ interactions with metal ions, resulting in the creation of metal phthalocyanines [17]. It is a big aromatic molecule with great chemical and thermal stability [18]. The anticancer

Check for updates

Academic Editors: Marilena Carbone, Qi Zhang and André F. Moreira

Received: 23 July 2026
Revised: 6 August 2026
Accepted: 14 August 2026
Published: 16 August 2026

**Copyright:** © 2026 by the authors. Licensee MDPI, Basel, Switzerland. This article is an open access article distributed under the terms and conditions of the Creative Commons Attribution (CC BY) license.

and antibacterial characteristics of phthalocyanines, especially metal derivatives like Zn, Al, Ga, Mg, and Cu complexes, have been extensively researched [18–20]. They function as photosensitizers in photodynamic treatment, causing cancer cells to die by producing reactive oxygen species when exposed to light ≈ 670–690 nm [4]. While reducing toxicity, structural alterations and nanoparticle encapsulation improve their tumor selectivity, cellular uptake, and therapeutic efficacy [4,21]. Similar to this, phthalocyanines have antibacterial activity against both Gram-positive and Gram-negative bacteria, through inducing membrane and DNA damage through reactive oxygen species (ROS) [22]. Their promise as multipurpose therapeutic agents is highlighted by nanoparticle encapsulation systems, which further enhance their solubility, stability, and cell penetration [23–25].

Drugs can be encapsulated in liposomes, nanoparticles [26,27], micelles, polymers, or hydrogels for active delivery [28]. Drug encapsulation is a vital strategy for targeted drug delivery, providing a protective shell or matrix around therapeutic compounds [9,24,28]. This approach enhances drug stability, enables controlled release, improves bioavailability, and reduces side effects, resulting in safer and more effective therapies [3,29,30]. Encapsulation and complex formation also protect sensitive bioactive substances from harsh environmental conditions, such as pH fluctuations, high temperatures, and enzymatic degradation [31,32]. Compared to conventional immediate-release formulations, it allows site-specific delivery, minimizes exposure to healthy tissues, and improves patient compliance while extending drug shelf life [28,33]. Natural low-density lipoprotein (LDL) exploits overexpressed LDL receptors on cancer cells for targeted uptake via receptor-mediated endocytosis [9,24,34]. Second, polyethylene glycol (PEG) synthetic nanoparticles improve circulation time, stability, and therapeutic efficacy, with several formulations already in clinical use passively entering the cells [35,36]. Third, chitosan, a natural polysaccharide, provides biocompatible, targeted nanoparticle passive delivery [37]. Together, these carriers enhance solubility, stability, cellular uptake, controlled release, and reduce toxicity [3,38,39]. In depth, encapsulating metal phthalocyanines in LDL, PEG, and chitosan nanoparticles enhances their anticancer and antibacterial activity by improving stability, cellular uptake, and passive delivery, enabling sustained nanozyme-mediated cytotoxic effects even in the absence of light [3,40–42].

Nanozymes are enzyme-mimicking nanomaterials that catalyze reactions cost-effectively and are widely used in diagnostics [43] and therapy, including anticancer and antibacterial applications [44,45]. Metal phthalocyanines, such as gallium and magnesium, exhibit nanozyme-like, ROS generation that induces cancer cell death, with some activity occurring even without light [46]. Recently Papadopoulos et al. showed that Ga(III) complexes are able to induce immunogenic cell death [47]. Similarly, other metal-based nanozymes (e.g., Au, Ag, $Fe_3O_4$, Cu, ZnO) facilitate ROS-mediated killing of tumor cells and bacteria [45,48,49]. Therefore, phthalocyanines encapsulated in nanoparticles demonstrate both direct and passive anticancer and antibacterial activity, even in the absence of light, due to their intrinsic chemical, catalytic, and nanozyme properties [49,50]. Iron, cobalt, copper, zinc, and manganese phthalocyanines generate ROS that cause DNA damage, mitochondrial dysfunction, and apoptosis in various cancer cells, while disrupting bacterial membranes and inhibiting enzymatic activity in *E. coli*, *S. aureus*, and *Pseudomonas aeruginosa* [51–53]. Encapsulation further enhances stability, cellular uptake, and sustained cytotoxicity [3], making metal phthalocyanine nanoparticles a promising platform for light-independent therapeutic applications [25].

In this project, we synthesized and fully characterized metal phthalocyanines mimicking the nanozyme activity using FAB-MS, NMR, UV–Vis, SEM, DLS, EDX, and TGA. After loading of the metal phthalocyanine into Chi, PEG, and LDL particles, the biological activi-

ties of these agents were evaluated against cancer cell lines (MDA-MB-453 and HEPG2) as well as *Escherichia coli* (*E. coli*) as a surrogate bacterial model, as represented in Figure 1.

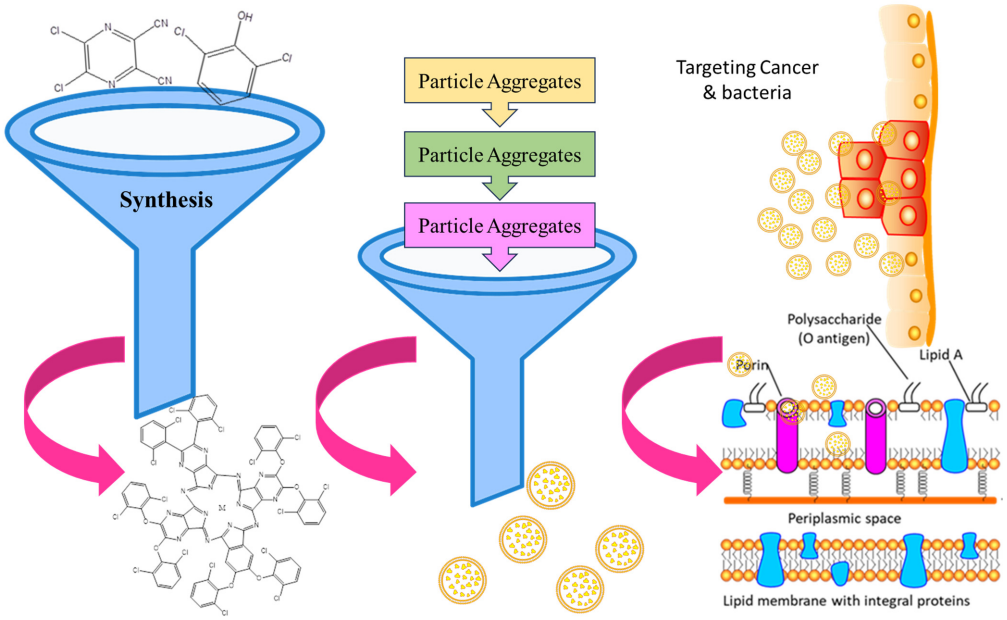



**Figure 1.** Metal phthalocyanines were synthesized and comprehensively characterized, followed by encapsulation and evaluation of their anticancer and antibacterial activities against cancer cell lines and *E. coli*.

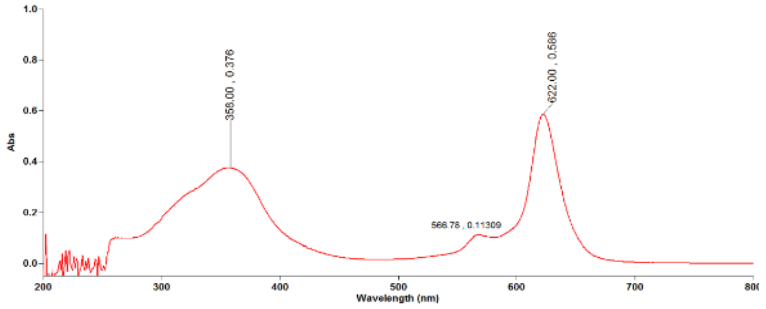
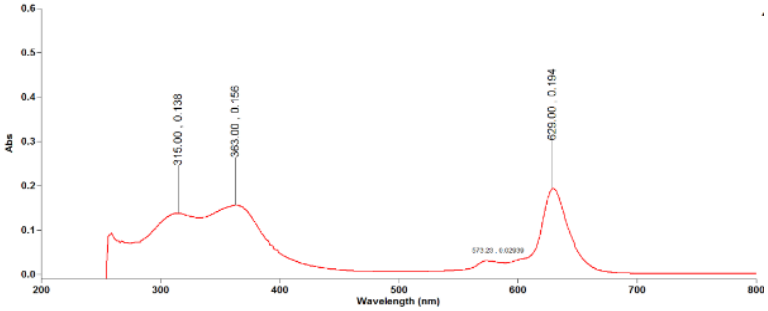
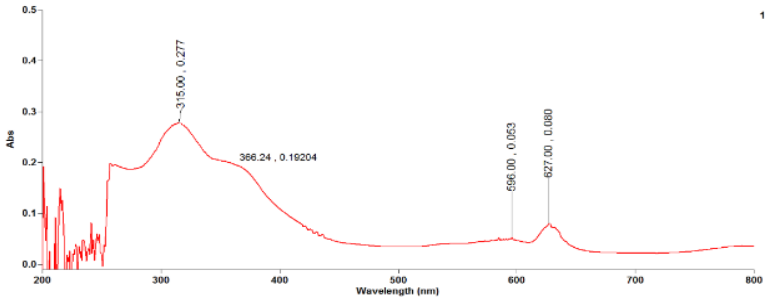
## 2. Results

Following synthesis, comprehensive physicochemical characterization and biological evaluations of the metals phthalocyanine agent were performed to demonstrate the ability of the metal phthalocyanine to enter cancer and bacterial cells and exert activity in the absence of light activation.

### *2.1. Electronic Absorption Spectral Analysis*

The UV–Vis spectra of all phthalocyanine agents exhibited distinct absorption peaks at around 350 nm and 650 nm [54], as summarized in Table 1. The absorption peaks of Cu phthalocyanine were at 358 and 622 nm, while Ga phthalocyanine showed absorption peaks at 315, 366 nm and 596–627 nm. Mg phthalocyanine absorption peaks were at 315–396, and 629 nm. In depth, the absorption peak near 330–370 nm is a B-band and originating from $\pi \rightarrow \pi^*$ electronic transitions within the conjugated phthalocyanine macrocycle. Its presence confirms the integrity and aromaticity of the phthalocyanine ring system. On the other hand, the strong absorption band observed in the 600–700 nm region is known as the Q-band. This band arises from $\pi \rightarrow \pi^*$ transitions involving the highest occupied molecular orbital (HOMO) and lowest unoccupied molecular orbital (LUMO) of the macrocycle [55,56]. Also, the exact position and intensity of the Q-band are influenced by the central metal ion, and this band is important because it lies in the visible to near-infrared region, making phthalocyanines suitable for applications in photodynamic therapy, photovoltaics, and sensors [57,58]. In sum, these bands confirmed the formation and the structural integrity of the metal phthalocyanine complexes. The structures were uniform even when increasing the concentrations ten times, as shown in Figure 2A,B. The spectra showed that phthalocyanine agents are in the monomeric form because even at high concentrations the data did not show broadening of the Q-band, reduction in the peak sharpness, or shift in the wavelength. Also based on the Beer–Lambert Law, the absorbance increases proportionally with the concentration [59].

**Table 1.** The UV–Vis absorption spectra of Cu, Mg, and Ga phthalocyanines were recorded in DMSO solvent over the wavelength range of 200–800 nm.

| Agent | Electronic Absorbance Spectra | Wavelength Range (nm) |
|---|---|---|
| Cu Phthalocyanine |  | Phthalocyanine 358–622 |
| Mg Phthalocyanine |  | Phthalocyanine 315, 366–596, 627 |
| Ga Phthalocyanine |  | Phthalocyanine 315, 396–627 |

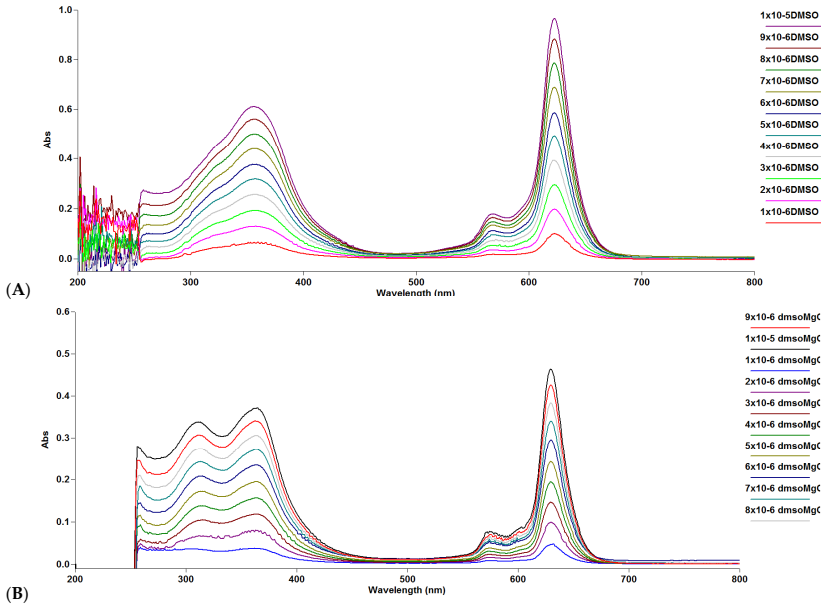
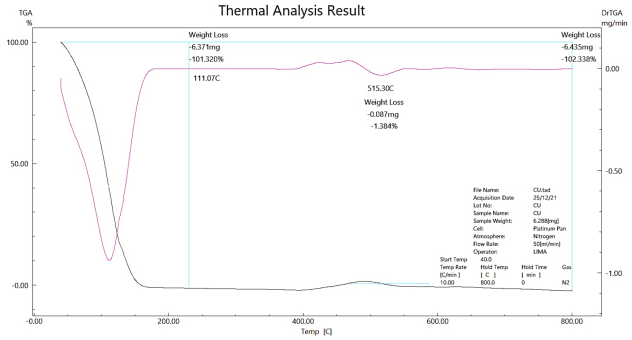
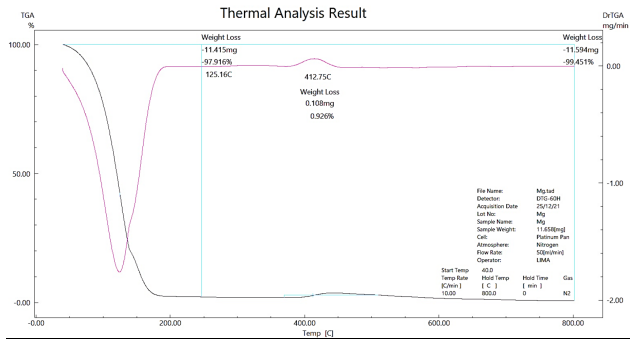
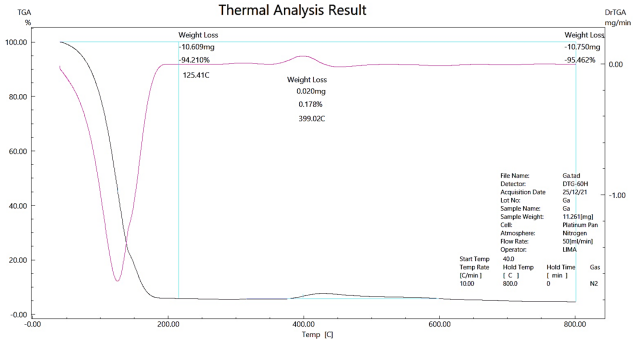



**Figure 2.** (**A**) Cu phthalocyanine and (**B**) Mg phthalocyanine showed consistent behavior across all tested doses, including a tenfold increase in concentration.

### *2.2. Evaluation of Thermal Stability Using TGA*

The purpose of thermal gravimetric analysis (TGA) is to compare agents' temperatures to 37 °C (normal body temperature), and it tells us whether the compound remains intact in the human body [60]. If there is weight loss close to or below 37 °C, the compound may be unstable under physiological conditions, which could reduce efficacy or cause premature degradation. The TGA data demonstrated distinct thermal degradation profiles for the synthesized metal phthalocyanines. Cu phthalocyanine exhibited the onset of thermal degradation at approximately 111 °C, whereas Mg and Ga phthalocyanines showed higher degradation temperatures, initiating at around 125 °C. The elevated decomposition temperatures of Mg and Ga phthalocyanines indicate superior thermal stability compared to the Cu analogue. Importantly, all compounds remained thermally stable well above 100 °C, which is significantly higher than physiological temperature (37 °C). This substantial thermal margin confirms that these phthalocyanine-based anticancer agents would retain their structural integrity under biological conditions, supporting their suitability for use as chemotherapy candidates (Table 2).

**Table 2.** Thermogravimetric assessment of phthalocyanine agents' stability under physiological conditions.

| Agent | TGA Thermogram (25–800 °C) |
| --- | --- |
| Cu Phthalocyanine |  |
| Mg Phthalocyanine |  |
| Ga Phthalocyanine |  |



Note: 37 °C, normal body temperature; 41 °C, high body temperature = fever.

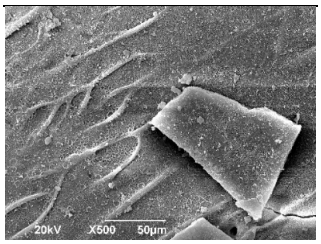
This wide thermal safety margin strongly suggests that the phthalocyanines will remain structurally intact under in vivo conditions, including during systemic circulation, cellular uptake, and intracellular localization [4]. Furthermore, such thermal stability is critical for maintaining chemical integrity during formulation processes such as encapsulation, sterilization, and storage [61]. Also, it reduces the likelihood of premature degradation or loss of therapeutic efficacy in biological environments. Collectively, these findings support the suitability of the synthesized metal phthalocyanines as stable anticancer candidates for in vivo chemotherapy applications [4]. In sum, TGA analysis revealed that metal phthalocyanines exhibit enhanced thermal stability compared to body temperature. Minor weight loss below 150 °C corresponds to the removal of adsorbed moisture, while a broad stable region extending up to ~350 °C indicates strong structural integrity. The main decomposition step at higher temperatures is associated with macrocyclic ring degradation. The higher decomposition onset temperatures and increased residual mass of the metal phthalocyanines confirm that metal insertion significantly improves thermal robustness through strong metal–nitrogen coordination [62].

### *2.3. EDX Spectroscopic Characterization of the Agents*

The energy-dispersive X-ray spectroscopy (EDX) identified and confirmed the presence of the elements in the sample in the analyzed area qualitatively and quantitatively. The samples were placed on double-face carbon tape and precoated with gold to enhance conductivity and signal quality. A comparison of the three phthalocyanine samples revealed that carbon was the dominant element in all cases, reflecting the aromatic and highly conjugated nature of the phthalocyanine macrocycle. Gallium phthalocyanine exhibited the highest carbon atomic percentage (88.13 at.%), followed by copper phthalocyanine (82.80 at.%) and magnesium phthalocyanine (69.44 at.%). Magnesium phthalocyanine was distinguished by a substantial nitrogen content (14.48 at.%), consistent with the nitrogen-rich structure of the phthalocyanine ring. The central metal atoms were detected in all samples, with copper showing the highest atomic percentage (1.21 at.%), followed by gallium (0.20 at.%) and magnesium (0.15 at.%). Overall, the elemental compositions are consistent with the expected characteristics of metal phthalocyanine materials, where a carbon-rich macrocyclic framework surrounds a centrally coordinated metal ion, as shown in Table 3.

**Table 3.** EDX measurements were conducted on Cu, Mg, and Ga phthalocyanine agents to determine the elemental percentages and overall weight contribution in the selected positions of the samples.

| Cu Phthalocyanine | Weight % | Atomic % |
|---|---|---|
| C | 65.29 | 82.80 |
| Cl | 23.48 | 10.09 |
| Cu | 5.03 | 1.21 |
| O | 6.20 | 5.90 |
| Total | 100 | 100 |



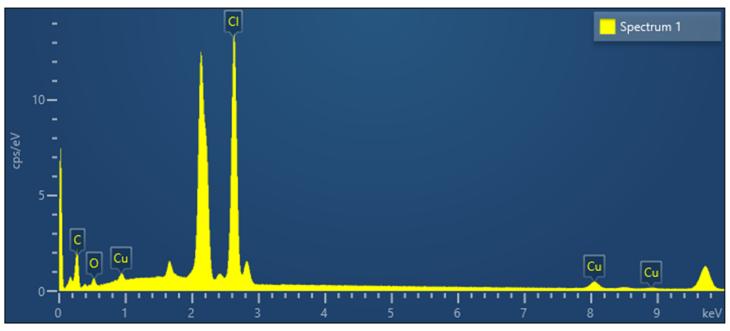
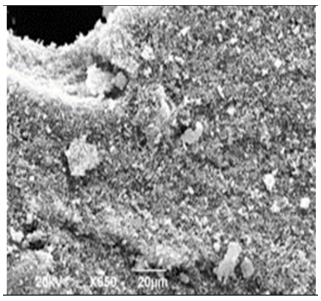
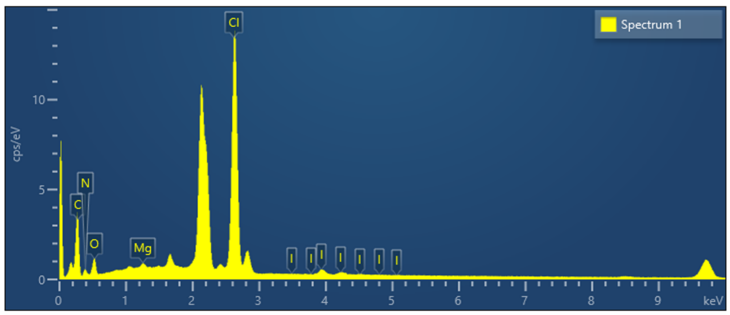



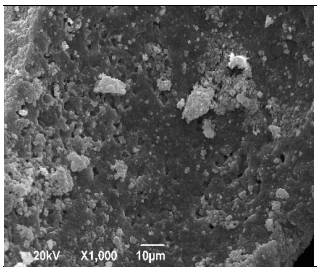
**Table 3.** *Cont.*

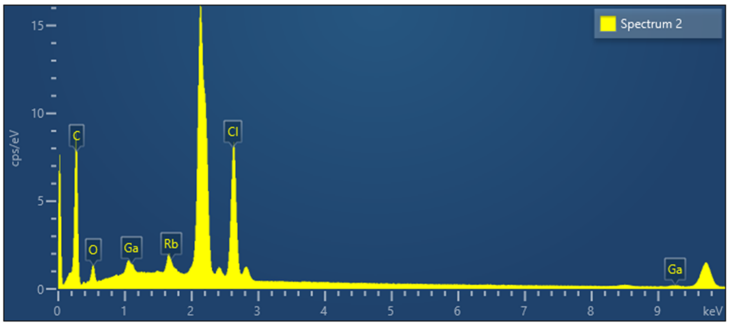
| Mg Phthalocyanine | Weight % | Atomic % |
|---|---|---|
| **C** | 57.61 | 69.44 |
| **Cl** | 16.61 | 6.78 |
| **O** | 9.90 | 8.96 |
| **N** | 14.01 | 14.48 |
| **Mg** | 0.25 | 0.15 |
| **I** | 1.61 | 0.18 |
| **Total** | 100 | 100 |






| Ga Phthalocyanine | Weight % | Atomic % |
|---|---|---|
| C | 79.54 | 88.13 |
| O | 9.83 | 8.18 |
| Cl | 9.12 | 3.42 |
| Ga | 1.07 | 0.20 |
| Rb | 0.43 | 0.07 |
| Total | 100 | 100 |

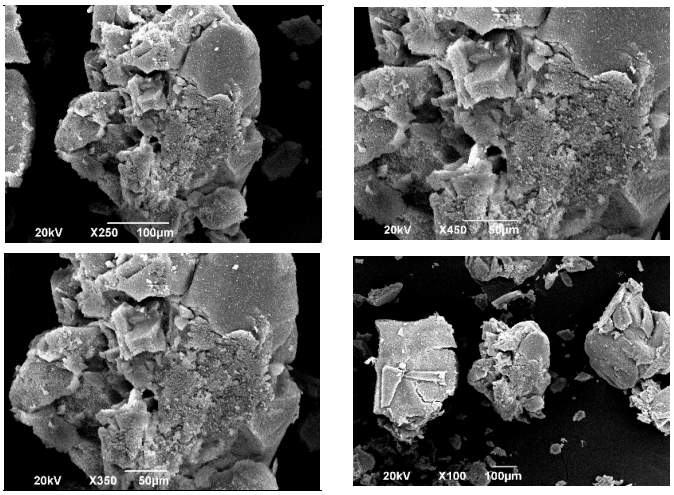
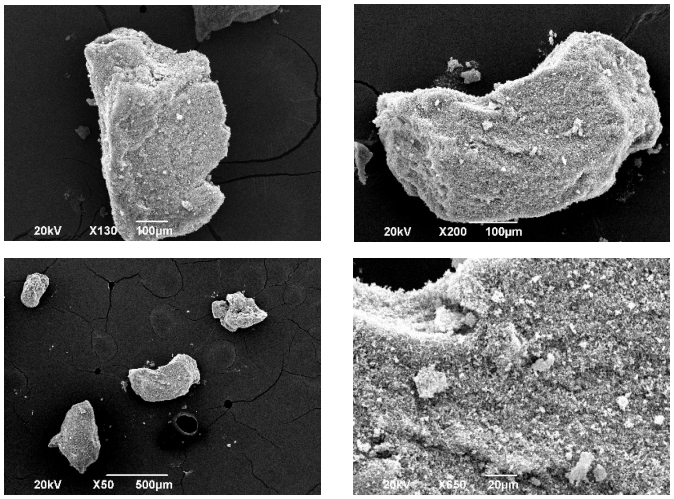
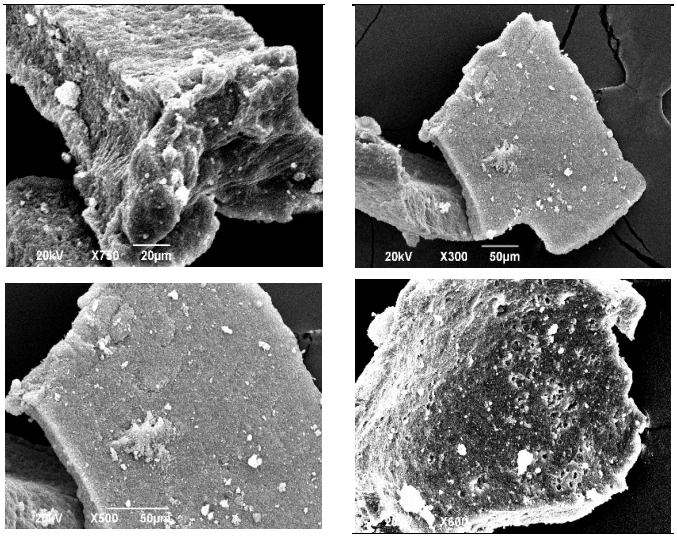



### *2.4. SEM Microscopy Data Analysis of the Metals Phthalocyanine Agents*

The micrographs of Cu, Mg and Ga phthalocyanine showed aggregates with rough and porous surfaces, as shown in Table 4. The data revealed that all agents were particle aggregates. Cu and Mg phthalocyanine morphologies were similar sharp and rough surfaces while Ga phthalocyanine showed sheet-like structures with the highest surface porosity. This porosity of the agents enables them to enhance the biological activity [63]. Porous materials are important in cancer therapy, as they can improve drug loading, facilitate tumor targeting, enable controlled release, and promote cellular uptake through both active and passive endocytosis, while also contributing directly to cancer cell killing through multiple mechanisms [64–66].

**Table 4.** SEM micrographs for the Cu, Mg, Ga phthalocyanine at different magnifications X50–X750 at 20, 50, 100, and 500 μM (at 20 kV).

| Agent/Structure | SEM Images |
| --- | --- |
| Cu Phthalocyanine Nanoparticles, sharp, rough surfaces. |  |
| Mg Phthalocyanine Nanoparticles, sharp, rough surfaces. |  |
| Ga Phthalocyanine Nanoparticles, porous, sheets surfaces. |  |

## *2.5. Metal Phthalocyanine Characterization*

Dynamic light scattering (Zeta sizer) analysis revealed that the synthesized agents exhibited varied morphologies capable of disrupting microtubule stability [3,66,67], with

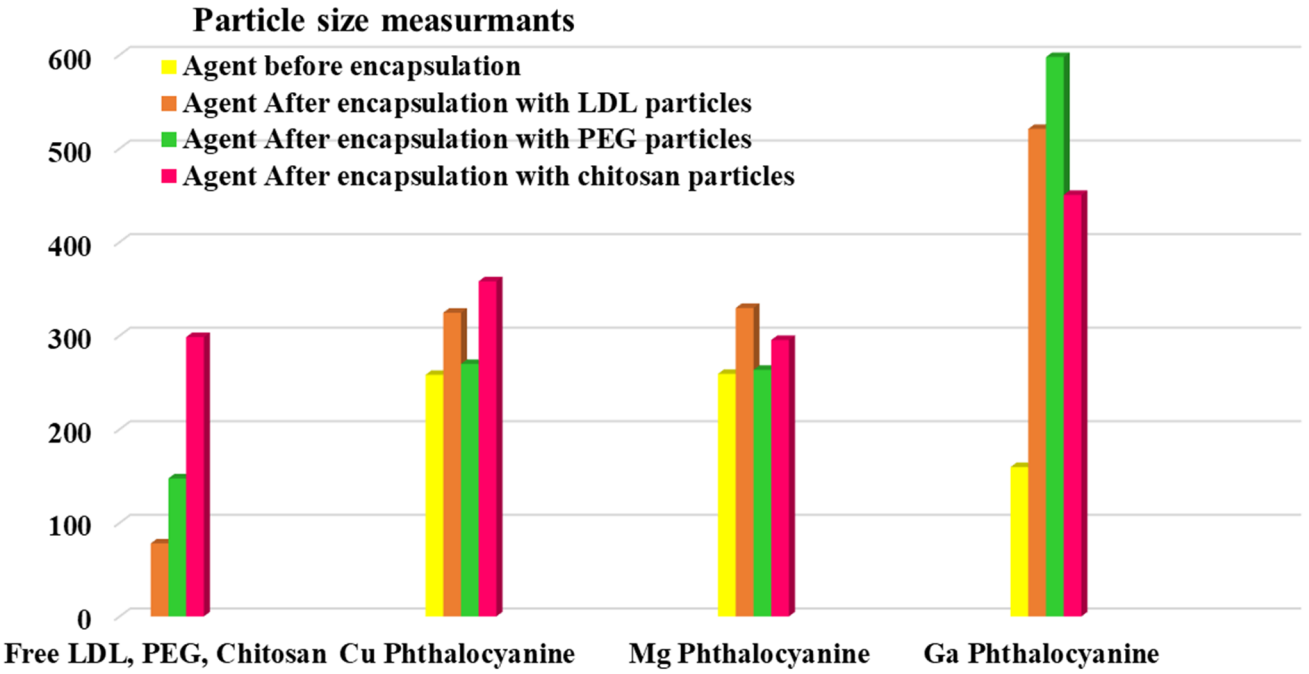
smaller forms such as clusters, sheet-like assemblies, and particles with sharp-edged or porous surfaces which have been reported to interact and interfere with cellular microtubules, potentially disrupting the stability of α- and β-tubulin subunits and thereby inhibiting proper mitotic spindle formation and preventing cell division [67–69]. Collectively, these physicochemical characteristics may enhance cellular uptake and biological efficacy, supporting the observed anticancer and antibacterial activities of the prepared particle aggregates.

### 2.6. Nanoparticle Size Distribution Analysis Before and After Complex Formation

Dynamic light scattering (DLS) analysis was performed to evaluate the hydrodynamic particle size, polydispersity index (PDI), and intensity distribution of the free phthalocyanines and their complexes with low-density lipoprotein (LDL), polyethylene glycol (PEG), and chitosan nanoparticles. The native carriers exhibited average particle sizes of 78.10 ± 3.57 nm for LDL, 147.5 ± 9.75 nm for PEG, and 298.5 ± 28.76 nm for Chi. The size distribution data are summarized in Table 5. The results revealed that all agents became bigger after Chi, PEG, and LDL aggregate formation [3,34–38]. In depth, all agents loaded with LDL became bigger than the free LDL [9,24]. This trend is the same with PEG and chitosan encapsulation compared to the free PEG and chitosan as controls. Following complex formation, the particle sizes increased in most formulations, indicating successful association of the phthalocyanines with the respective nanocarriers. Cu phthalocyanine increased from 258.1 ± 64.74 nm to 324.5 ± 22.59 nm with LDL, 269.7 ± 28.42 nm with PEG, and 358.1 ± 24.71 nm with chitosan. Similarly, Mg phthalocyanine increased from 259.2 ± 66.86 nm to 329.6 ± 20.60 nm with LDL, while particle sizes of 263.4 ± 36.99 nm and 295.3 ± 3.82 nm were observed after complexation with PEG and chitosan, respectively. Among all formulations, Ga phthalocyanine exhibited the greatest increase in particle size, increasing from 159.5 ± 38.11 nm to 520.9 ± 95.74 nm with LDL, 597.7 ± 94.30 nm with PEG, and 450.4 ± 21.24 nm with chitosan, suggesting stronger interactions with the carrier matrices and a greater tendency toward nanoparticle aggregation.

The poly dispersive index (PDI) values revealed differences in particle size uniformity among the formulations. Native LDL exhibited a moderate PDI of 0.382, whereas free PEG and chitosan showed broader size distributions with PDIs of 1.000. Following complex formation, the PDI values ranged from 0.339 to 0.946, indicating varying degrees of particle homogeneity. The Ga-LDL formulation exhibited the lowest PDI (0.339), suggesting a comparatively more uniform particle population despite its larger particle size, while Cu-chitosan (0.920), Mg-LDL (0.932), and Ga-chitosan (0.946) displayed broader size distributions, indicative of greater heterogeneity and possible aggregation. The intensity-weighted distributions demonstrated that most formulations were dominated by a single particle population (100% intensity), confirming the formation of the desired particle complexes. However, Cu-PEG (71% intensity) and Ga-PEG (55% intensity) exhibited additional particle populations, indicating the coexistence of particles with different sizes or the presence of aggregates. As DLS intensity distributions are strongly influenced by larger particles, these lower-intensity percentages likely reflect minor aggregated populations rather than a reduction in particle formation. Overall, the DLS results confirm successful complexation of the phthalocyanines with LDL, PEG, and chitosan carriers, with gallium phthalocyanine producing the largest hydrodynamic particle sizes and the greatest influence on particle size distribution.

**Table 5.** DLS measurements of Cu, Mg, and Ga phthalocyanines were performed in water.

| Agent | Size of Agent Before Complex Formation | Agent Size After Complex Formation with LDL Particles DPI (Intensity) | Agent Size After Complex Formation with PEG Particles DPI (Intensity) | Agent Size After Complex Formation with Chitosan Particles DPI (Intensity) |
|---|---|---|---|---|
|  | | | | |
| Free LDL, PEG, Chitosan | - | 78.10 ± 3.569<br>0.382 (49) | 147.5 ± 9.748<br>1.000 (100) | 298.5 ± 28.76<br>1.000 (100) |
| Cu Phthalocyanine | 258.1 ± 64.74<br>0.510 (100) | 324.5 ± 22.59<br>0.787 (100) | 269.7 ± 28.42<br>0.397 (71) | 358.1 ± 24.71<br>0920 (100) |
| Mg Phthalocyanine | 259.2 ± 66.86<br>1.000 (82) | 329.6 ± 20.60<br>0.932 (100) | 263.4 ± 36.99<br>0651 (100) | 295.3 ± 3.815<br>0.604 (100) |
| Ga Phthalocyanine | 159.5 ± 38.11<br>0.482 (100) | 520.9 ± 95.74<br>0.339 (100) | 597.7 ± 94.30<br>0.806 (55) | 450.4 ± 21.24<br>0.946 (100) |



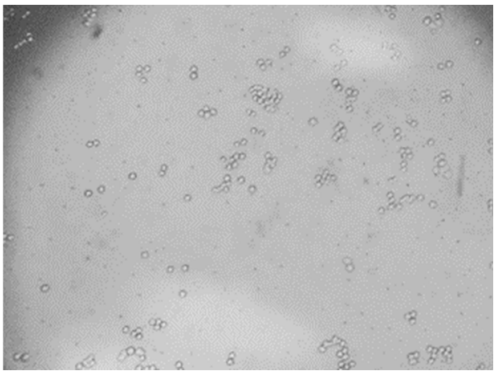
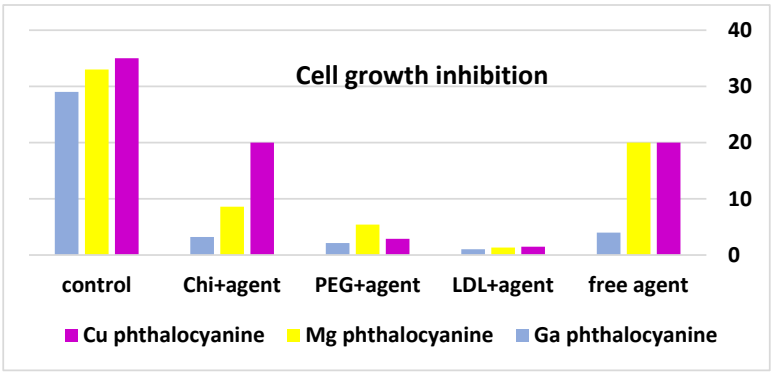
The particle size average diameter (nm) ± standard deviation. PDI < 0.10 (highly monodisperse). PDI 0.10–0.30 (narrow distribution). PDI 0.30–0.50 (moderate distribution). PDI > 0.50 (broad or heterogeneous distribution).

### *2.7. Quantitative Analysis of MTT Assay Results*

The cytotoxic effects of Cu, Mg, and Ga phthalocyanines and their particle-based formulations were evaluated against the MDA-MB-453 breast cancer cell line, with HEK293 normal human cells serving as a non-cancerous control. All the culture results are summarized in Table 6. The data revealed that Cu and Mg phthalocyanine did not show potent cell growth inhibition when treated with breast cancer cell line at 25 μM, while Ga phthalocyanine showed potent cancer cell growth at 3.965 ± 0.097 μM $IC_{50}$ value against breast cancer cells. The results demonstrated that particle formulation significantly enhanced the anticancer activity of all tested phthalocyanines, as evidenced by substantial reductions in $IC_{50}$ values compared with the free compounds. As lower $IC_{50}$ values indicate greater cytotoxic potency, the LDL-loaded formulations consistently exhibited the strongest anticancer effects among the tested delivery systems [3]. First, loading of the agents with LDL showed that Ga > Mg > Cu. Second, loading of the agents with PEG showed that Ga > Cu > Mg. Third, loading with chitosan showed the same trend as LDL Ga > Mg > Cu. For Cu phthalocyanine, the free compound displayed relatively weak activity against MDA-MB-453 cells, with an $IC_{50}$ value exceeding 20 μM. However, encapsulation within LDL nanoparticles markedly improved its cytotoxic efficacy, reducing the $IC_{50}$ to

1.478 ± 0.144 μM. PEG loading also enhanced activity, yielding an $IC_{50}$ of 2.86 ± 0.113 μM, whereas chitosan loading did not produce a comparable improvement, with the $IC_{50}$ remaining above 20 μM. These findings indicate that LDL-mediated delivery substantially increased the intracellular effectiveness of Cu phthalocyanine, likely through enhanced cellular uptake by breast cancer cells. A similar trend was observed for Mg phthalocyanine. The free compound exhibited limited cytotoxicity, with an $IC_{50}$ value exceeding 20 μM. Following LDL encapsulation, the $IC_{50}$ decreased dramatically to 1.319 ± 0.151 μM, representing the most pronounced enhancement among the Mg-based formulations. PEG loading also improved activity, although to a lesser extent ($IC_{50}$ = 5.402 ± 0.120 μM), while chitosan loading produced an intermediate effect with an $IC_{50}$ of 8.597 ± 0.120 μM. These results demonstrate that particle-mediated delivery significantly potentiates the anticancer activity of Mg phthalocyanine, with LDL particles providing the greatest enhancement. Among all compounds investigated, Ga phthalocyanine exhibited the highest intrinsic anticancer activity. The free compound achieved an $IC_{50}$ value of 3.965 ± 0.097 μM, which was considerably lower than those of free Cu and Mg phthalocyanines. Incorporation into LDL nanoparticles further enhanced its potency, producing the lowest $IC_{50}$ value observed in the entire study (1.030 ± 0.112 μM). PEG and chitosan formulations also improved cytotoxicity, yielding $IC_{50}$ values of 2.114 ± 0.143 μM and 3.207 ± 0.104 μM, respectively. The superior activity of Ga phthalocyanine suggests that the gallium center contributes favorably to biological interactions and cellular toxicity toward breast cancer cells, while LDL encapsulation maximizes its therapeutic efficacy.

**Table 6.** The $IC_{50}$ data of the treated breast cancer cells with Cu, Mg, Ga phthalocyanine at concentration of 25 μM.

| MDA-MB-453 | $IC_{50}$ Values Agent Treatment at 25 μM | $IC_{50}$ Values Agent Loaded LDL Treatment 25 μM | $IC_{50}$ Values Agent Loaded PEG Treatment 25 μM | $IC_{50}$ Values Agent Loaded Chitosan Treatment 25 μM | $IC_{50}$ Values Agent Treatment with HEK293 at 25 μM |
|---|---|---|---|---|---|
|  | |   | | | |
| Cu phthalocyanine | >20 | 1.478 ± 0.144 | 2.86 ± 0.113 | >20 | 35.11 ± 0.142 |
| Mg phthalocyanine | >20 | 1.319 ± 0.151 | 5.402 ± 0.120 | 8.597 ± 0.120 | 33.24 ± 0.514 |
| Ga phthalocyanine * | 3.965 ± 0.097 | 1.030 ± 0.112 | 2.114 ± 0.143 | 3.207 ± 0.104 | 29.36 ± 0.215 |

*: The most potent. LDL best drug delivery (LDL > PEG > chitosan). MDA-MB-453 = breast cancer cell line. HEK293 = healthy cells used as control. Agents loaded to carrier (1:5 ratio).

The data revealed that LDL complex formation showed potent $IC_{50}$ values when breast cancer cells were treated with all metal phthalocyanine agents followed by PEG encapsulation then chitosan nanoparticles. This enhanced efficacy may be attributed to the elevated expression of low-density lipoprotein receptors (LDLRs) on many breast cancer cells, including MDA-MB-453 cells, which facilitate receptor-mediated endocytosis and selective accumulation of LDL-associated therapeutic agents within malignant tissues.

Consequently, LDL nanoparticles appear to provide a targeted delivery mechanism that enhances intracellular drug concentration and therapeutic response.

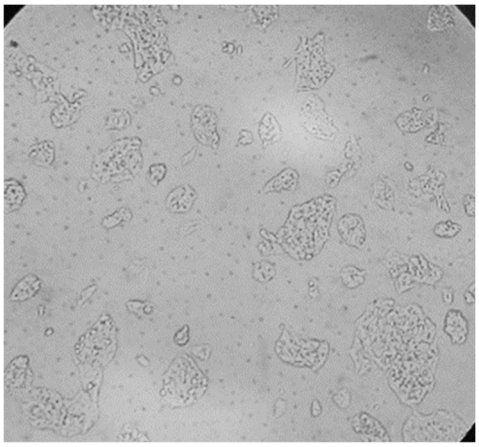
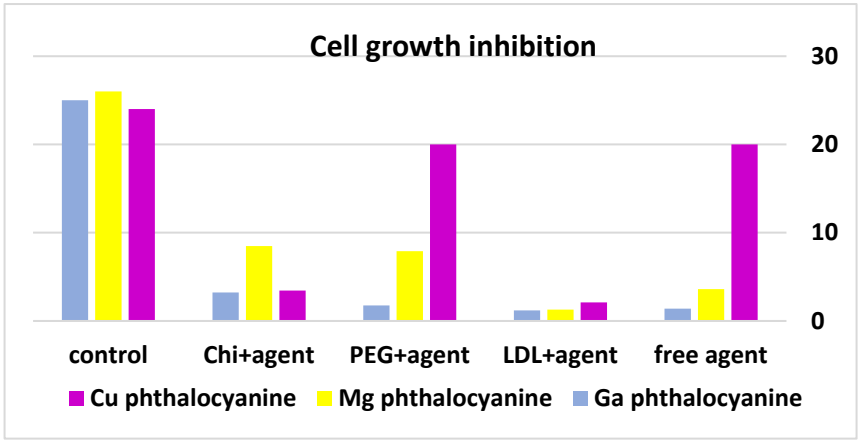
Evaluation of cytotoxicity toward HEK293 normal cells further demonstrated favorable selectivity for cancer cells. The free phthalocyanines exhibited substantially higher $IC_{50}$ values against HEK293 cells, ranging from 29.36 ± 0.215 to 35.11 ± 0.142 μM, compared with their corresponding $IC_{50}$ values in MDA-MB-453 cells. Ga phthalocyanine, despite being the most potent anticancer agent, maintained an $IC_{50}$ of 29.36 ± 0.215 μM in HEK293 cells, indicating a wide therapeutic window. The approximate selectivity indices (HEK293 $IC_{50}$/MDA-MB-453 $IC_{50}$) for the free compounds were >1.75 for Cu phthalocyanine, >1.66 for Mg phthalocyanine, and 7.41 for Ga phthalocyanine, demonstrating particularly strong cancer cell selectivity for the gallium derivative.

Overall, the data identify Ga phthalocyanine as the most potent anticancer agent, while LDL nanoparticles represent the most effective drug delivery system. The LDL-loaded Ga phthalocyanine formulation exhibited the greatest cytotoxic activity against MDA-MB-453 cells, achieving an $IC_{50}$ of 1.030 ± 0.112 μM, nearly fourfold lower than that of the free compound. These findings suggest that combining gallium phthalocyanine with LDL-mediated delivery may represent a promising strategy for targeted breast cancer therapy, offering enhanced anticancer efficacy while maintaining a favorable selectivity profile toward normal cells.

The anticancer activities of Cu, Mg, and Ga phthalocyanines and their corresponding particle formulations were evaluated against the HepG2 liver cancer cell line, while HEK293 cells were used as a normal cell control to assess selectivity. The results demonstrated that both the nature of the central metal ion and the choice of nanocarrier significantly influenced cytotoxic efficacy. Overall, LDL-based formulations consistently produced the lowest $IC_{50}$ values, confirming their superior drug delivery performance, whereas Ga phthalocyanine emerged as the most potent anticancer agent among the investigated compounds. The substantial differences between the $IC_{50}$ values obtained for HepG2 and HEK293 cells further indicate a favorable therapeutic profile toward malignant cells, the data summarized in Table 7. First, loading of the agents with LDL showed the same trend as the breast cancer treatment: Ga > Mg > Cu. Second, loading of the agents with PEG also showed that Ga > Cu > Mg. Third, loading with chitosan showed the same trend as LDL loading: Ga > Mg > Cu [70]. All complex formation had an agent to carrier ratio of 1:5. Cu phthalocyanine exhibited relatively weak intrinsic activity against HepG2 cells, with an $IC_{50}$ value exceeding 20 μM when administered in its free form. However, encapsulation within nanocarriers markedly improved its cytotoxic performance. LDL-loaded Cu phthalocyanine demonstrated the greatest enhancement, reducing the $IC_{50}$ to 2.108 ± 0.111 μM, while PEG and chitosan formulations yielded $IC_{50}$ values of 3.450 ± 0.109 μM and 8.610 ± 0.111 μM, respectively. These findings indicate that particle-mediated delivery substantially increases the biological effectiveness of Cu phthalocyanine, with LDL particles producing approximately a tenfold improvement in activity relative to the free compound. The enhanced efficacy may be attributed to improved cellular internalization and more efficient intracellular drug accumulation. Mg phthalocyanine displayed considerably greater intrinsic cytotoxicity than Cu phthalocyanine, exhibiting an $IC_{50}$ value of 3.616 ± 0.110 μM against HepG2 cells. Loading in LDL particles further enhanced its activity, resulting in an $IC_{50}$ of 1.296 ± 0.111 μM. In contrast, PEG- and chitosan-based formulations produced $IC_{50}$ values of 7.906 ± 0.136 μM and 8.483 ± 0.100 μM, respectively, both of which were less effective than the free compound. This observation suggests that while LDL particles significantly improve the delivery and potency of Mg phthalocyanine, PEG and chitosan matrices may reduce its bioavailability or alter its interaction with cancer cells. Nevertheless, the LDL-loaded Mg phthalocyanine formulation remained among the

most effective treatments evaluated, demonstrating nearly a threefold increase in potency relative to the free drug. Ga phthalocyanine exhibited the strongest intrinsic anticancer activity against HepG2 cells, achieving an $IC_{50}$ value of 1.401 ± 0.101 µM. This potency was further enhanced following LDL complex formation, producing the lowest $IC_{50}$ value observed in the study (1.193 ± 0.102 µM). PEG loading maintained a high level of activity, with an $IC_{50}$ value of 1.754 ± 0.103 µM, whereas chitosan loading resulted in a moderate reduction in efficacy ($IC_{50}$ = 3.221 ± 0.130 µM). The consistently low $IC_{50}$ values observed for all Ga phthalocyanine formulations indicate that the gallium-centered phthalocyanine possesses strong inherent cytotoxic properties and remains highly effective regardless of the delivery platform. The slight but measurable improvement achieved through LDL complex formation suggests that the compound already possesses excellent cellular accessibility, while LDL delivery provides an additional enhancement in therapeutic efficiency.

**Table 7.** The $IC_{50}$ data of treated liver cancer cells with Cu, Mg, Ga phthalocyanine at concentration of 25 µM.

| HEPG2 | $IC_{50}$ Values Agent Treatment at 25 µM | $IC_{50}$ Values Agent Loaded LDL Treatment 25 µM | $IC_{50}$ Values Agent Loaded PEG Treatment 25 µM | $IC_{50}$ Values Agent Loaded Chitosan Treatment 25 µM | $IC_{50}$ Values Agent Treatment with HEK293 at 25 µM |
|---|---|---|---|---|---|
|  | |   | | | |
| Cu phthalocyanine | >20 | 2.108 ± 0.111 | 3.450 ± 0.109 | 8.610 ± 0.111 | 24.01 ± 0.327 |
| Mg phthalocyanine | 3.616 ± 0.110 | 1.296 ± 0.111 | 7.906 ± 0.136 | 8.483 ± 0.100 | 26.22 ± 0.429 |
| Ga phthalocyanine * | 1.401 ± 0.101 | 1.193 ± 0.102 | 1.754 ± 0.103 | 3.221 ± 0.130 | 24.32 ± 0.485 |

*: The most potent. LDL = best drug delivery. HEPG2 = liver cancer cell line. HEK293 = healthy cells used as control. Agents loaded to carrier (1:5 ratio).

Comparison of the three delivery systems revealed a clear trend in anticancer performance. LDL particles consistently produced the lowest $IC_{50}$ values for all phthalocyanines, confirming their superiority as drug carriers. PEG formulations generally showed intermediate effectiveness, whereas chitosan-based formulations produced the highest $IC_{50}$ values in most cases. The superior performance of LDL particles may be related to receptor-mediated uptake mechanisms, as cancer cells often exhibit increased lipid requirements and elevated expression of LDL receptors to support rapid proliferation [39]. Consequently, LDL-associated phthalocyanines can be internalized more efficiently, resulting in higher intracellular drug concentrations and enhanced cytotoxic activity [71]. LDL entered both cancer cells through binding to the LDL receptor like a key and lock [3,72]. In sum, LDL nanoparticles were the most potent complex formation strategy that entered the cells and caused cancer cell death.

Assessment of cytotoxicity toward HEK293 cells demonstrated that all three phthalocyanines were substantially less toxic to normal cells than to HepG2 cancer cells. The

$IC_{50}$ values against HEK293 cells ranged from 24.01 ± 0.327 to 26.22 ± 0.429 μM, considerably higher than those recorded for HepG2 cells. Ga phthalocyanine exhibited an $IC_{50}$ of 24.32 ± 0.485 μM in HEK293 cells compared with 1.401 ± 0.101 μM in HepG2 cells, corresponding to an approximate selectivity index of 17.4 (healthy cells/cancer cells). Similarly, Mg phthalocyanine demonstrated a selectivity index of approximately 7.3, while Cu phthalocyanine exhibited a selectivity index greater than 1.2 due to its lower intrinsic activity against HepG2 cells. These findings indicate that Ga phthalocyanine possesses the most favorable balance between potency and selectivity, producing strong cytotoxic effects in cancer cells while maintaining comparatively low toxicity toward healthy cells.

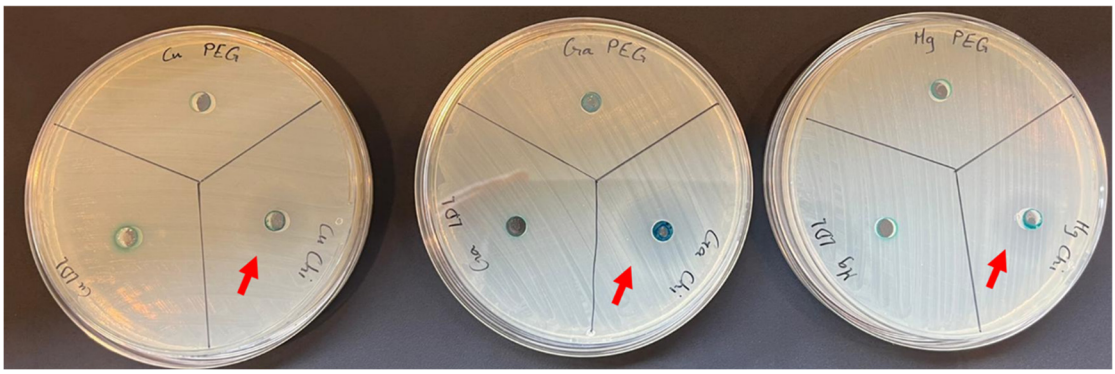
Overall, the results identify Ga phthalocyanine as the most potent anticancer agent against HepG2 liver cancer cells, owing to its exceptionally low $IC_{50}$ values in both free and formulated forms. Furthermore, LDL particles were the most effective delivery system, consistently enhancing the cytotoxic activity of all tested phthalocyanines. The LDL-loaded Ga phthalocyanine formulation achieved the greatest anticancer efficacy, with an $IC_{50}$ value of 1.193 ± 0.102 μM, while retaining a wide therapeutic margin relative to HEK293 cells. These findings highlight the potential of gallium phthalocyanine, particularly when delivered through LDL nanoparticles, as a promising candidate for targeted liver cancer therapy.

### *2.8. In Vitro Antibacterial Evaluation of Metal Phthalocyanines*

The antibacterial activity of Cu, Mg, and Ga phthalocyanines, both in their free form and following encapsulation within LDL, PEG, and chitosan carriers, was evaluated against *Escherichia coli* using the agar diffusion method. The antibacterial experimental data is summarized in Table 8. The results demonstrated generally low antibacterial activity for all tested formulations, as evidenced by the absence of distinct inhibition zones in most treatments. Free Cu, Mg, and Ga phthalocyanines did not produce detectable inhibitory effects against *E. coli* at 10 μM, indicating that the agents alone were unable to effectively suppress bacterial growth under the experimental conditions employed. Similarly, LDL and PEG formulations failed to generate measurable inhibition zones at 10 μM, suggesting that these delivery systems did not significantly enhance the antibacterial efficacy of the phthalocyanines against this Gram-negative bacterium. In contrast, chitosan formulations exhibited detectable, although limited, antibacterial activity. Chitosan-loaded Cu phthalocyanine produced an inhibition zone of 1.8 mm, while chitosan-loaded Mg phthalocyanine generated a slightly smaller zone of 1.6 mm at 10 μM. The most pronounced antibacterial response was observed for chitosan-loaded Ga phthalocyanine, which produced an inhibition zone of 2.2 mm at 10 μM. Despite these measurable effects, the inhibition zones were described as weak and poorly defined, indicating only marginal suppression of bacterial growth. The absence of clear inhibition boundaries suggests that the antibacterial action was insufficient to produce strong bactericidal or bacteriostatic effects when using low concentration of the agents. The superior performance of the chitosan-based formulations relative to LDL and PEG carriers may be attributed to the intrinsic antimicrobial properties of chitosan. As a positively charged biopolymer, chitosan can interact electrostatically with the negatively charged bacterial cell envelope, increasing membrane permeability and disrupting normal cellular functions. This interaction may facilitate closer contact between the complex phthalocyanines and bacterial cells, thereby enhancing antibacterial activity. Nevertheless, the small inhibition zones observed indicate that the contribution of chitosan was limited and that the overall susceptibility of *E. coli* to these formulations remained low [70].

**Table 8.** Antibacterial activity of metal phthalocyanine agents at 10 μM concentration.

| Agent/*E. coli* | Free Agents (Control) | Agents Loaded with LDL 10 μM (Diameter-mm) | Agents Loaded with PEG 10 μM (Diameter-mm) | Agents Loaded with Chitosan 10 μM (Diameter-mm) |
|---|---|---|---|---|
| Cu phthalocyanine | Nill | Nill | Nill | 1.8 * |
| Mg phthalocyanine | Nill | Nill | Nill | 1.6 * |
| Ga phthalocyanine | Nill | Nill | Nill | 2.2 * |




* Weak bacterial inhibition zone, not clear zones. The results are an average of three runs. *E. coli* is prokaryotic cells (Gram-negative bacteria). The diameter was measured by ruler.

Among the tested compounds, Ga phthalocyanine exhibited the greatest antibacterial activity when delivered through chitosan nanoparticles, followed by Cu and Mg phthalocyanines. This trend may reflect differences in the physicochemical properties of the central metal ions, which can influence interactions with bacterial membranes and intracellular targets. However, the relatively small differences among the inhibition zones suggest that the type of carrier had a more pronounced influence on antibacterial performance than the specific phthalocyanine derivative itself. The limited antibacterial efficacy observed against *E. coli* is consistent with the well-documented resistance of Gram-negative bacteria to many antimicrobial agents. The outer membrane of *E. coli*, which contains lipopolysaccharides, acts as an effective permeability barrier that restricts the penetration of large molecules and aggregates-associated agents. Consequently, the phthalocyanine formulations were largely unable to reach intracellular targets at concentrations sufficient to produce substantial bacterial inhibition. Overall, the findings indicate that while chitosan encapsulation provided a modest enhancement in antibacterial activity, all tested formulations exhibited only weak inhibitory effects against *E. coli*, with chitosan-loaded Ga phthalocyanine representing the most active formulation among those evaluated.

To further evaluate the antibacterial potential of the synthesized metal phthalocyanines, *E. coli* cultures were exposed to higher treatment concentrations. At 50 μM, a substantial enhancement in antibacterial activity was observed for all tested formulations. The inhibition zone diameters for Cu, Mg, and Ga phthalocyanines ranged from 1.3 to 3.0 cm, 1.2 to 2.9 cm, and 1.3 to 3.0 cm, respectively, indicating a concentration-dependent increase in bacterial growth inhibition. Further increasing the concentration to 70 μM resulted in an even greater antibacterial response, with inhibition zone diameters expanding to 1.7–3.4 cm for Cu phthalocyanine, 1.7–3.2 cm for Mg phthalocyanine, and 2.0–3.5 cm for Ga phthalocyanine. Among the investigated compounds, Ga phthalocyanine exhibited the strongest antibacterial performance at the highest concentration tested.

The observed increase in inhibition zone diameter with increasing concentration demonstrates a clear dose-dependent antibacterial effect of the metal phthalocyanines against *E. coli*. Moreover, loading formulations consistently exhibited superior antibacterial activity compared with their free counterparts, highlighting the effectiveness of the carrier

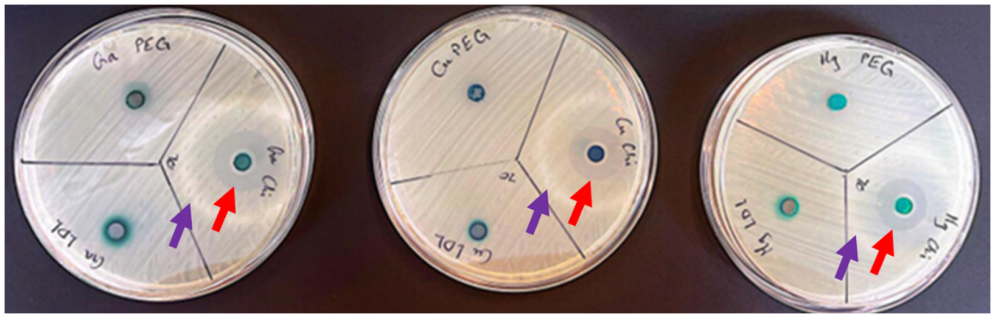
systems in enhancing the biological performance of these agents [30,32,34]. Improved dispersion, increased surface interaction with bacterial cells, and enhanced delivery of the active agents likely contributed to the observed enhancement in antibacterial efficacy. Collectively, these findings demonstrate that metal phthalocyanines, particularly when incorporated into carrier systems, possess significant antibacterial potential, and can produce pronounced and well-defined growth inhibition against *E. coli* at elevated concentrations (Table 9) [36,39].

**Table 9.** The antibacterial activity of the synthesized metal phthalocyanine agents was evaluated against a representative Gram-negative bacterial strain, revealing concentration-dependent inhibitory effects even in the absence of light activation.

| **Encapsulated with Chitosan 50 µM Concentration** | | |
|---|---|---|
| **Clear Inhibition Zone** | | **Weak Inhibition Zone** |
| Cu phthalocyanine | 1.3 cm | 3.0 cm |
| Mg phthalocyanine | 1.2 cm | 2.9 cm |
| Ga phthalocyanine | 1.3 cm | 3.0 cm |



| **Encapsulated with Chitosan 70 µM** | | |
|---|---|---|
| **Clear Inhibition Zone** | | **Weak Inhibition Zone** |
| Cu phthalocyanine | 1.7 cm | 3.4 cm |
| Mg phthalocyanine | 1.7 cm | 3.2 cm |
| Ga phthalocyanine * | 2.0 cm | 3.5 cm |



* *E. coli*: Gram-negative bacteria, potent. Values represent inhibition zone diameters measured after treatment with chitosan-encapsulated Cu, Mg, and Ga phthalocyanines at concentrations of 50 and 70 µM using a ruler. The clear inhibition zone corresponds to the region of complete bacterial growth suppression, whereas the weak inhibition zone represents the surrounding area of partial growth inhibition. Larger inhibition zone diameters indicate greater antibacterial activity. *Escherichia coli* is a Gram-negative bacterial strain commonly used for evaluating antimicrobial efficacy. Among the tested compounds, Ga phthalocyanine exhibited the strongest antibacterial activity, particularly at 70 µM, where the largest clear and overall inhibition zones were observed.

## 3. Discussion

Metal phthalocyanines have traditionally been investigated as photosensitizers for photodynamic therapy because of their strong absorption in the visible and near-infrared regions and their ability to generate reactive oxygen species (ROS) upon light activation. However, increasing evidence suggests that selected metallophthalocyanines may also exert biological activity in the absence of external irradiation through redox-mediated processes, disruption of intracellular homeostasis, and metal-dependent biochemical interactions, additionally inhibiting iron-dependent pathways due to $Fe^{3+}$ mimicry [45,49,73]. In the present study, we demonstrate that Cu-, Mg-, and particularly Ga-phthalocyanine formulations possess significant anticancer activity under dark conditions, and that nanoencapsulation within LDL, PEG, and chitosan carriers substantially enhances their biological performance [74–77]. These findings expand the therapeutic potential of phthalocyanine-based systems beyond conventional photodynamic applications and support their development as multifunctional nanotherapeutics.

The physicochemical characterization data provide important insights into the observed biological activities. UV–Vis spectroscopy confirmed preservation of the characteristic B and Q bands of the phthalocyanine macrocycle, indicating successful synthesis and structural integrity of the metal complexes [55]. Importantly, the absence of significant spectral broadening at elevated concentrations suggests limited aggregation and preservation of monomeric species, a feature often associated with improved biological performance and more predictable cellular interactions. Furthermore, TGA analysis demonstrated high thermal stability, with decomposition temperatures substantially exceeding physiological conditions, indicating that the complexes are likely to remain structurally intact during circulation, cellular uptake, and intracellular trafficking. Such stability is particularly important for therapeutic applications because premature degradation can compromise bioavailability and reduce therapeutic efficacy [3,60].

Further, the EDX spectroscopy qualitatively and quantitatively confirmed the agents' components [3]. SEM and DLS analyses revealed particle aggregates possessing rough and porous surface morphologies. These structural characteristics are increasingly recognized as important determinants of nanomedicine performance Porous architectures provide greater surface area for biological interactions, facilitate adsorption to cellular membranes, and may enhance intracellular accumulation through endocytic pathways [9,24]. In addition, porosity can kill cancer cells via several mechanisms: either drug delivery, photothermal therapy or gene delivery. Also, porous compounds can target DNA, RNA, and induce apoptosis [78]. Moreover, studies have shown that porous particles can target *E. coli* bacteria through a combination of physiochemical surface modifications such as liposaccharides, positive selective binding, and responsive release mechanism such as acidic pH or enzyme sensitive linkers [79], and the advantages are controlled release, reduced resistance development, high loading capacity of the drug, and improved solubility and stability [80]. For example, mesoporous silica nanoparticles functionalized with cationic polymers and loaded with silver ions have been shown to selectively bind to *E. coli* cell walls and kill them via membrane disruption and ROS production [81]. Furthermore, nanoparticles offer significant advantages in cancer therapy and antibacterial applications due to their unique properties [26,27]. In cancer, they enable targeted drug delivery, improve solubility and stability, allow controlled release, and enhance cellular uptake, reducing systemic toxicity [3,28]. Also, in antibacterial studies, nanoparticles can disrupt bacterial membranes, induce oxidative stress, overcome antibiotic resistance, provide targeted delivery, and penetrate biofilms that are typically resistant to conventional antibiotics [82–84].

The marked increase in hydrodynamic diameter following incorporation into LDL, PEG, and chitosan carriers confirms successful formulation and suggests strong interactions

between the phthalocyanines and carrier matrices. Notably, gallium II phthalocyanine produced the largest particle size increases after complex formation, indicating stronger carrier association and potentially improved cellular retention. Such characteristics may partially explain the superior biological activity observed for the gallium II phthalocyanine formulations.

Among the investigated compounds, gallium phthalocyanine consistently exhibited the highest anticancer activity against both MDA-MB-453 breast cancer and HepG2 liver cancer cells [85]. The superior efficacy of the gallium derivative may originate from several complementary mechanisms. Gallium shares chemical similarities with ferric iron ($Fe^{3+}$) and can interfere with iron-dependent cellular processes that are essential for tumor proliferation. Rapidly growing cancer cells exhibit elevated iron requirements for DNA synthesis, mitochondrial function, and metabolic activity [86]. Consequently, intracellular gallium accumulation can disrupt iron metabolism, inhibit ribonucleotide reductase activity, induce oxidative stress, and, ultimately, trigger apoptosis. These mechanisms likely act synergistically with the intrinsic redox properties of the phthalocyanine scaffold, producing enhanced cytotoxic effects even in the absence of photoactivation. The exceptionally low $IC_{50}$ values observed for gallium phthalocyanine therefore suggest that the metal center itself contributes significantly to biological activity rather than serving solely as a structural component of the macrocycle.

A particularly important finding of this study is the substantial enhancement in anticancer activity achieved through complex formation. Across both cancer models, LDL-based formulations consistently produced the lowest $IC_{50}$ values, outperforming PEG and chitosan carriers [34,36,39]. This observation is consistent with the metabolic demands of malignant cells, which frequently overexpress LDL receptors to support increased cholesterol uptake required for membrane biosynthesis and rapid proliferation [9,24]. Exploiting this biological pathway enables receptor-mediated endocytosis and preferential intracellular delivery of LDL-associated therapeutics. The nearly fourfold improvement observed for LDL-loaded gallium II phthalocyanine in breast cancer cells and the similarly enhanced activity in HepG2 cells strongly support this targeting mechanism. These findings are particularly relevant because they demonstrate that naturally occurring lipoproteins can function as efficient and potentially biocompatible drug-delivery vehicles for metallo phthalocyanine-based therapeutics.

Although PEGylated formulations generally improved anticancer activity relative to the free compounds, their performance remained inferior to LDL-based systems. PEG is known to improve colloidal stability, reduce opsonization, and prolong systemic circulation; however, it lacks the active targeting capability provided by LDL-receptor-mediated uptake [39]. Consequently, the observed improvements are likely attributable primarily to enhanced solubility and cellular exposure rather than selective tumor targeting. Chitosan formulations produced variable responses depending on the metal center, suggesting that electrostatic interactions alone may be insufficient to maximize intracellular delivery of all phthalocyanine derivatives. These observations highlight the importance of matching carrier properties to both the physicochemical characteristics of the therapeutic agent and the biological features of the target cells.

An additional strength of the present work is the favorable selectivity observed toward cancer cells compared with HEK293 normal cells. Gallium II phthalocyanine displayed the highest selectivity indices among all tested agents, indicating that enhanced potency was not accompanied by proportional toxicity toward non-malignant cells. Such selectivity is a critical requirement for clinical translation because many conventional chemotherapeutics exhibit severe dose-limiting toxicities resulting from poor discrimination between healthy and malignant tissues. The combination of strong cytotoxic activity and relatively low

toxicity toward normal cells suggests that gallium II phthalocyanine-based formulations may possess a therapeutically advantageous safety profile.

The antibacterial findings provide further evidence of the multifunctional nature of these formulations. At low concentrations, antibacterial activity against *Escherichia coli* was limited, with measurable inhibition observed primarily for chitosan-loaded formulations. The enhanced performance of chitosan-containing systems is consistent with the established antimicrobial properties of chitosan, which can interact with negatively charged bacterial membranes, increase membrane permeability, and facilitate delivery of encapsulated agents [25,86–91]. At higher concentrations, all formulations exhibited concentration-dependent antibacterial activity, with gallium II phthalocyanine again demonstrating the strongest response. The superior antibacterial performance of gallium-containing systems may be explained by disruption of bacterial iron acquisition pathways, a mechanism analogous to its effects in cancer cells. As iron is essential for bacterial metabolism and replication, gallium can function as a non-functional iron mimic, interfering with iron-dependent enzymatic processes and impairing bacterial survival [89]. Phthalocyanine-encapsulated nanoparticles exhibited pronounced light-independent anticancer and antibacterial activity [25], extending their utility beyond photodynamic therapy. Complex formation strategy enhanced stability, cellular uptake, and passive targeting, while biological effects were driven by redox disruption, mitochondrial dysfunction, and membrane destabilization [90]. These results establish phthalocyanine-based nanoplatforms as promising dual-function agents for oncology and antimicrobial applications [91].

The observation of biological activity in the absence of light activation represents one of the most significant aspects of this work. Most phthalocyanine-based studies focus primarily on photodynamic mechanisms, whereas the current findings suggest that appropriately engineered metallo phthalocyanine formulations can retain substantial biological activity under dark conditions [20–22]. This characteristic could potentially overcome some of the major limitations of photodynamic therapy, including restricted light penetration, dependence on external irradiation, and reduced effectiveness against deep-seated tumors. Consequently, these formulations may represent a new generation of phthalocyanine-based therapeutics capable of functioning through both photoactivated and non-photoactivated pathways.

For better drug delivery, the metal phthalocyanines were loaded into different carriers. LDL particles selectively target cancer cells due to the overexpression of LDL receptors on tumor cells, facilitating receptor-mediated uptake and enhanced intracellular drug delivery [3,34,92]. Also, PEGylation improves nanoparticle stability and prolongs systemic circulation, enabling passive accumulation within tumor tissues through the enhanced permeability and retention effect [93]. In addition, chitosan nanoparticles exhibit enhanced affinity toward cancer cells due to electrostatic interactions with negatively charged cell membranes and increased uptake under acidic tumor microenvironment conditions, and this was proved by the MTT assay [3,34,94].

In sum, Ga phthalocyanine showed potent anticancer and antibacterial activities because of its porosity surface, nanosized particles, and metal effect, which cause cell disruption without light activation [9,24,88,95]. In short, this study demonstrates that gallium (Ga II) phthalocyanine can efficiently enter cells when encapsulated within carriers, highlighting the critical role of complex formation in enhancing cellular uptake.

Despite these promising findings, several limitations should be acknowledged. First, the study was restricted to in vitro cancer and bacterial models, and therefore the in vivo pharmacokinetics, biodistribution, toxicity, and therapeutic efficacy remain to be established. Second, direct mechanistic investigations of ROS generation, apoptosis induction, mitochondrial dysfunction, and iron-metabolism disruption were not performed and

should be included in future studies to confirm the proposed mechanisms. Third, only a single Gram-negative bacterial strain was evaluated, and broader antimicrobial testing against clinically relevant Gram-positive and multidrug-resistant pathogens would provide a more comprehensive assessment of antibacterial potential. Finally, quantitative measurements of loading efficiency, drug release kinetics, and receptor-mediated uptake would further strengthen understanding of the relationship between formulation properties and biological activity.

Overall, the present study demonstrates that encapsulated metallo phthalocyanines, particularly gallium II phthalocyanine, possess significant light-independent anticancer and antibacterial activity. The combination of favorable physicochemical characteristics, enhanced efficacy following complex formation, strong selectivity toward cancer cells, and dual therapeutic functionality highlights gallium II phthalocyanine complex formation as promising candidates for future translational development. Further mechanistic and in vivo investigations are warranted to validate these findings and advance this platform toward clinical application.

## 4. Materials and Methods

### *4.1. Chemicals*

Sigma-Aldrich (Burlington, MA, USA) provided all the chemicals utilized for synthesis, anticancer and antibacterial research, and no additional preparation was required such as 5,6-dichloro-2,3-dicyanopyrazin, 2,6-dichlorophenol, acetonitrile, anhydrous potassium carbonate, quinoline, hexane, ethyl acetate, $MgCl_2$, $GaCl_2$, pentanol, DBU, Copper acetate, DMSO, polyethylene glycol (PEG 202398-Sigma Aldrich), chitosan powder (low-molecular-weight 448869—Sigma Aldrich), LDL (LDL serum-S5519), DMEM media, FBS, penicillin/streptomycin, 1% L-glutathione, PBS, and the WST-1 assay kit (ab65473, Abcam—Sigma Aldrich). The tested organism *E. coli* (strain SL06/16-1 16S ribosomal RNA gene with accession number KX279366) was obtained from the Department of Biology, College of Science, Kuwait University.

### *4.2. Instruments*

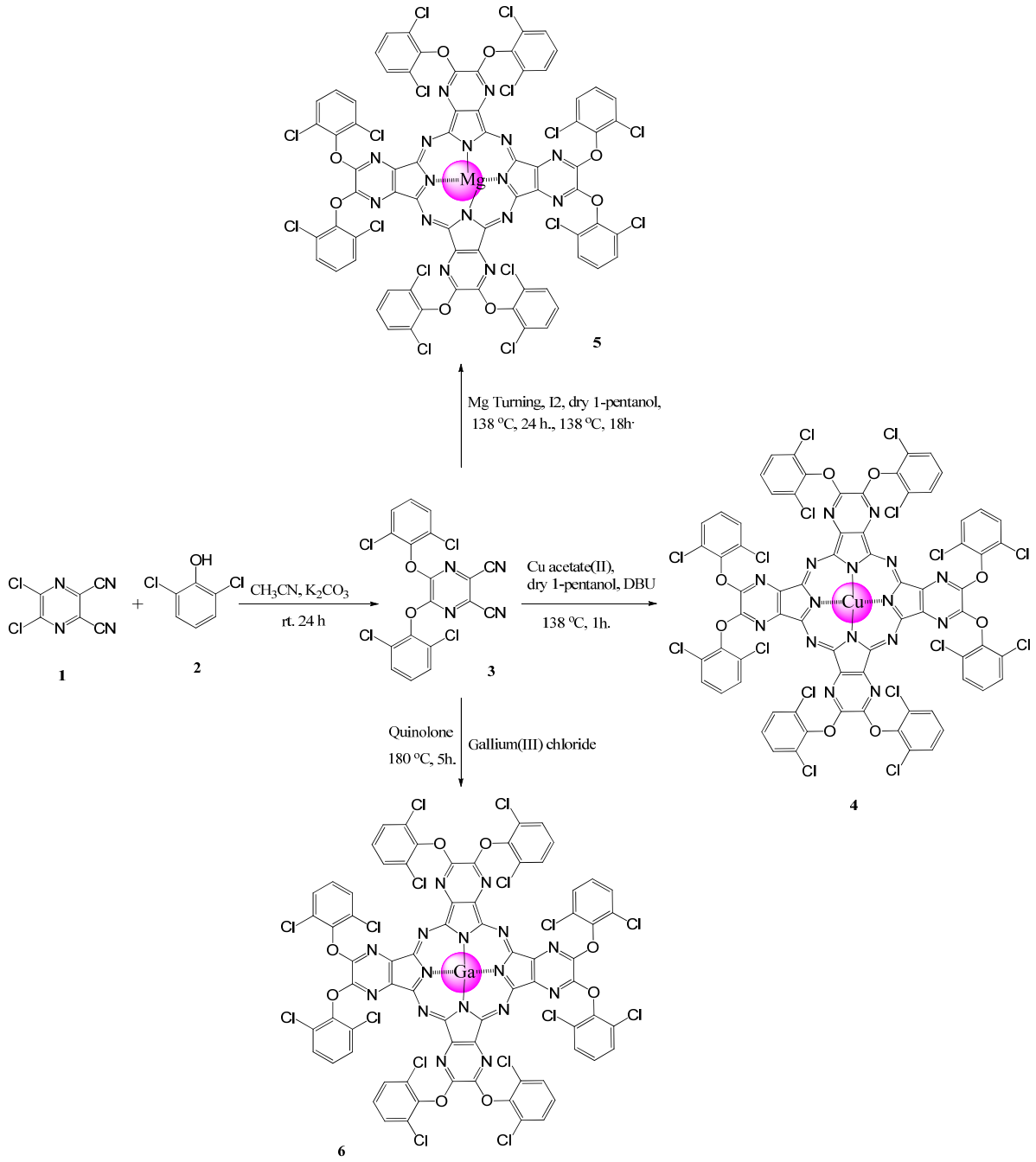
All spectral analysis was carried out at Kuwait University's Research Sector Project Unit (RSPU). FAB-MS (Thermos-6000 by Thermo Fisher Scientific, (Thermos LLC, Wiesbaden, Germany), a high-resolution gas chromatograph mass spectrometer–double focusing (GC-MS) DFS model, was used to quantify the samples' molecular weight. A Bruker DPX 600 NMR spectrophotometer (Bruker, Billerica, MA, USA) was used to collect $^1H$ nuclear magnetic resonance (NMR) spectra at 600 MHz in DMSO and $CDCl_3$. A UV–Vis spectrophotometer performed optical spectroscopy, a technique used to study how light interacts with matter in the ultraviolet (UV) and visible (Vis) regions of the electromagnetic spectrum (UVVIS NIR-AGILENT CARY 5000). Elemental analysis (CHNS) was carried out using an elemental uni-cube superuser.

### *4.3. Synthesis of the Metal Phthalocyanine Agent and Characterization*

Previously, we synthesized and fully characterized Mg and Cu phthalocyanine agents in our laboratories at Kuwait University. The process of creating 5,6-dichloro pyrazine-2,3-dicarbonitrile (**3**) is described in [96].

Ga phthalocyanine production started as shown in Scheme 1, by stirring a mixture of 5,6-dichloropyrazine-2,3-dicarbonitrile (1) (1 equiv.) with 2,6-dichlorophenol (2) (2.1 equiv.) in 10 mL of dry acetonitrile solvent and anhydrous potassium carbonate (5 equiv.) as catalyst. The reaction mixture was stirred at room temperature in a nitrogen environment for 24 h. Then, 5,6-bis(2,6-dichlorophenoxy)pyrazine-2,3-dicarbonitrile (**3**) was obtained

by reducing the reaction solvent by evaporation, washing the crude product many times with distilled water, and then air drying it. After that, we heated a mixture of compound (**3**) (500 mg, 1.10 mmol) with gallium chloride (44 mg, 0.276 mmol), and quinoline (3 mL) to 180 °C in a nitrogen environment for five hours. Then, nitrobenzene (2.00 mL) was added. After two hours of continuous heating, the temperature was lowered to 120 °C. Following cooling, an n-hexane: ethyl acetate (1:1, $v/v$) solvent mixture was added as an eluent in column chromatography on silica gel to purify the crude product known as (2,3,9,10,16,17,23,24-Octakis(2,6-dichlorophenoxy)azaphthalocyaninato Gallium).




**Scheme 1.** Schematic presentation of the synthesis procedures to obtain the metal phthalocyanine agents (Ga II, Cu II, Mg II).

Melting point: N300 °C; yield: 100 mg (19.30%); Ms.: 1864.844 (M+), 1519.705, 1034.498. Elemental analysis Calc. (%) for $C_{72}H_{24}Cl_{16}N_{16}O_8Ga$: C, 46.05; H, 1.29; N, 11.93; Found: C,

46.11, H, 1.30; N, 11.94; $^{1}$H NMR (DMSO d6, 600 MHz) δ/ppm = 7.39–7.95 (m, 24 H) as shown in the Supplementary Materials.

It is important to note that $^{13}$C NMR spectra could not be obtained for gallium phthalocyanine due to severe line broadening induced by the quadrupolar nature of the gallium nucleus and the strong Ga–N coordination within the macrocyclic framework, which leads to rapid relaxation of nearby carbon nuclei and loss of spectral resolution. In addition, although gallium phthalocyanine is diamagnetic, the quadrupolar nature of the gallium nucleus ($^{69}$Ga and $^{71}$Ga, I = 3/2) induces rapid relaxation and severe line broadening of nearby $^{13}$C nuclei, rendering the $^{13}$C NMR signals undetectable [97].

### *4.4. UV–Visible Spectroscopic Analysis*

A UV–Vis spectrophotometer provides information about the electronic transitions in molecules, especially conjugated systems like interactions of phthalocyanines with light in UV–Vis regions [55,98]. It helps confirm the formation of the compound and its structural features. In a UV–Vis spectrophotometer, light from a deuterium (UV) or halogen (Vis–NIR) source passes through sample and reference cuvettes. The sample absorbs specific wavelengths, and the transmitted light is measured by a photomultiplier tube (PMT). Absorbance is proportional to concentration according to the Beer–Lambert law, producing a spectrum across the UV and visible regions [9,99].

### *4.5. TGA-Based Thermal Stability Assessment*

Thermogravimetric analysis (TGA) offered insights into the thermal stability and water content of the metal phthalocyanine agents. Also, TGA allows comparison of thermal stability between materials, evaluation of effect of additives, coatings, or encapsulation, and prediction of material performance under heat. Approximately 5 mg of each agent was placed in a platinum pan and heated under a nitrogen atmosphere from 25 to 800 °C for 10 min. The measured weight reduction and the computed complex composition were clearly correlated, according to the results [3,60].

### *4.6. EDX Characterization and SEM Imaging of the Metal Phthalocyanine*

The surface morphology and elemental composition of the synthesized materials were characterized using scanning electron microscopy (SEM) coupled with energy-dispersive X-ray spectroscopy (EDX, JEOL, Tokyo, Japan). EDX is a powerful analytical technique that provides both qualitative and quantitative information regarding the elemental composition and distribution of materials. When integrated with SEM, it enables localized elemental analysis of specific regions and surface features, allowing comprehensive physicochemical characterization of the samples [60]. SEM imaging was performed using a JEOL CarryScope JSM-5700 scanning electron microscope, while elemental analysis was conducted using a JEOL Flash 1400 EDX detector [9,24].

SEM analyses were carried out at an accelerating voltage of 20.0 kV, and micrographs were obtained at various magnifications (×50, ×100, ×130, ×200, ×250, ×300, ×350, ×450, ×500, ×600, ×650, and ×750). Samples prepared at concentrations of 20, 50, 100, and 500 µM were examined to evaluate their morphological characteristics. The acquired micrographs were used to assess particle size, shape, surface texture, roughness, porosity, aggregation behavior, and the presence of structural features such as cracks or fissures. The combined SEM–EDX approach enabled correlation between surface morphology and elemental composition, providing valuable insight into the structural properties of the investigated materials [60].

Prior to analysis, powder samples were mounted onto aluminum stubs using double-sided conductive adhesive tape to ensure adequate sample fixation. The mounted specimens were subsequently coated with a thin layer of gold using a Leica EM ACE200

(Germany by Leica Microsystems, Wetzlar, Germany) sputter coater to improve electrical conductivity and minimize charging effects during electron beam exposure. All SEM and EDX analyses were conducted at the Research and Scientific Projects Unit (RSPU), and the resulting images and spectra were used to evaluate the morphological and elemental characteristics of the synthesized materials [68].

### 4.7. Complex Formation of Metal Phthalocyanines

Low-density lipoprotein (LDL; Sigma-Aldrich, S5519), polyethylene glycol (PEG; Sigma-Aldrich, CAS No. 25322-68-3, average molecular weight Mn 400, hydroxyl-terminated), and chitosan (Chi; Sigma-Aldrich, CAS No. 9012-76-4, low molecular weight) were used as received without further preparation. To prepare the chitosan solution, acetic acid was diluted in distilled water to obtain 1% $v/v$. Subsequently, one gram of chitosan powder was gradually added to 100 mL of the solution under continuous stirring at 50–60 °C until a homogeneous and transparent solution was obtained. The pH of the chitosan solution was adjusted to approximately 5.5–6.0 using 0.1 M NaOH to improve polymer stability and facilitate particle aggregates formation. The resulting LDL, PEG, and chitosan preparations were used as particle carriers in the liquid phase.

Next, for complex formation, 50 µL of each metal phthalocyanine was incorporated and mixed with 250 µL particles using pipetting, vortex mixing, and sonication at a 1:5 agent-to-particle ratio (1:5 $v/v$), as shown in Figure 3. The mixtures were initially homogenized by pipetting and vortex mixing for 5 min, followed by sonication in an ultrasonic bath for 45–60 min at room temperature (28 ± 2 °C) to promote uniform dispersion and enhance interactions between the phthalocyanine molecules and the carrier systems. The resulting suspensions were further homogenized using a Polytron dispersing and mixing device (Kinematica AG, Lucerne, Switzerland) and then incubated overnight (24 h) at 4 °C to facilitate complex formation reorganization and efficient loading of the metal phthalocyanines. The same procedure was applied to all investigated agents, while unloaded LDL, PEG, and chitosan particles were prepared under identical conditions and used as controls [3,9,28,29,100]. Following preparation, all formulations were stored in sterile, amber-colored containers at 4 °C to protect the samples from light-induced degradation and maintain physicochemical stability. Samples were kept under refrigerated conditions and used within one week of preparation to minimize potential changes in particle size, loading efficiency, and biological activity. Prior to characterization or biological assays, the formulations were gently vortexed to ensure uniform dispersion.

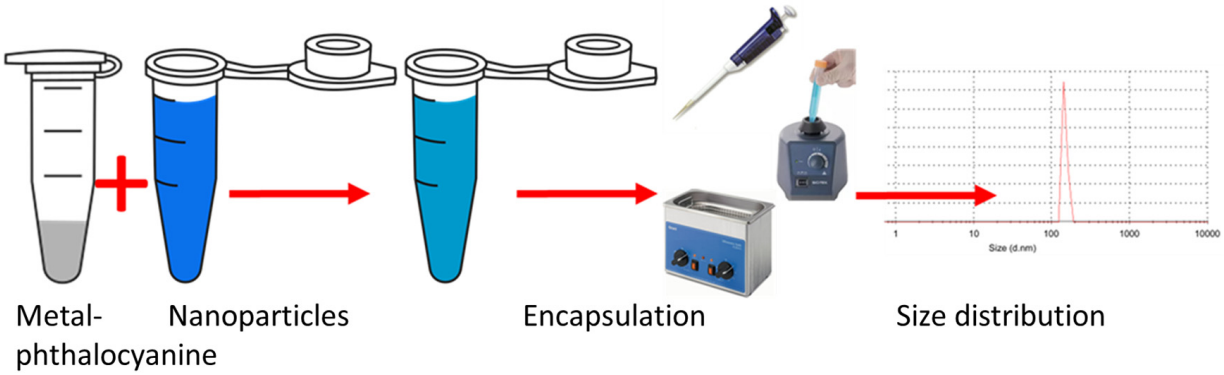



**Figure 3.** Schematic representation of nanoparticle preparation and complex formation: the metal phthalocyanine solution is mixed and pipetted into the particle matrix, followed by sonication for one hour. The resulting particles are analyzed using DLS to determine their size distribution.

### 4.8. Dynamic Light Scattering Measuring the Particles' Size

Particle size distribution and zeta potential measurements were determined using a Malvern Zetasizer Nano ZS (Malvern Panalytical Ltd., Great Malvern, Worcestershire, UK), which operates based on dynamic light scattering and electrophoretic light scattering (ELS) principles. DLS was employed to determine the hydrodynamic diameter and size distribution of the nanoparticles, while ELS was used to evaluate surface charge (zeta potential), an important indicator of colloidal stability. The instrument is capable of measuring particle sizes ranging from 0.3 nm to 10 µm and incorporates automatic temperature control to ensure measurement accuracy and reproducibility. All analyses were performed at the Research Sector Projects Unit (RSPU), Kuwait University. Prior to measurement, 100 µL of free nanoparticles (LDL, PEG, and chitosan) or metal-phthalocyanine-loaded particle formulations were diluted with deionized water to obtain an appropriate scattering intensity and prevent multiple scattering effects. The samples were gently vortexed and subsequently sonicated in an ultrasonic bath for 5 min at room temperature (25 ± 2 °C) to ensure complete dispersion and minimize particle aggregation. Following sonication, the suspensions were transferred into disposable polystyrene cuvettes for particle size measurements. All measurements were conducted at pH 7.0, and samples were allowed to equilibrate within the instrument for 2 min before data acquisition.

Particle size measurements were performed at a scattering angle of 173° (backscatter detection mode) and a controlled temperature of 25 °C. For each sample, three independent measurements were obtained, with each measurement consisting of multiple runs to ensure reproducibility. The average hydrodynamic diameter and polydispersity index (PDI) values were recorded and expressed as mean ± standard deviation (SD). These parameters were used to evaluate particle size distribution, dispersion homogeneity, and colloidal stability before subsequent physicochemical and biological analyses [3,60,101].

### 4.9. Cell Culture

Dulbecco's Modified Eagle Media (DMEM-D0822, Sigma Aldrich and Merck, Darmstadt, Germany) was supplemented with 10% FBS, 1% penicillin/streptomycin, and 1% L-glutathione. FBS was inactivated in a water bath at 37 °C for 30 min before being used. All reagents were purchased from Sigma-Aldrich and ready for direct use without further preparation [9,24].

### 4.10. Assessment of Cell Proliferation Induced by Metal Phthalocyanine Agents

The cytotoxic effects of the synthesized compounds and their nanoparticle formulations were evaluated using the MTT assay, a widely employed colorimetric method for assessing cell viability and proliferation based on mitochondrial metabolic activity in viable cells [68,102]. Human liver carcinoma (HepG2) and human breast carcinoma (MDA-MB-453) cell lines were cultured under standard conditions and maintained in complete growth medium supplemented with fetal bovine serum and antibiotics. Cells were seeded into 96-well microplates at a density of $1 \times 10^5$ cells/well and incubated overnight at 37 °C in a humidified atmosphere containing 5% $CO_2$ to allow cell attachment and stabilization. The plates were then incubated for 2 h at 37 °C to allow viable cells to reduce the yellow tetrazolium salt into insoluble purple formazan crystals, followed by the addition of 100 µL of MTT solution after the removal of the old media and incubated for two hours. Next, the addition of 100 µL dimethyl sulfoxide (DMSO) was accompanied by ten minutes of shaking to ensure complete solubilization. Absorbance was subsequently measured at 450 nm using a microplate reader (Gen5, Molecular Devices, Dasman Diabetes Institute, Kuwait city, Kuwait). Cell viability was calculated relative to untreated control cells, and

all treatments were performed in quadruplicate. Results are expressed as mean ± standard deviation (SD) from independent experiments [103].

### 4.11. Statistical Analysis

Statistical analyses were performed using GraphPad Prism version 9.0 (GraphPad Software, San Diego, CA, USA). All experiments were conducted in quadruplicate, and the results are presented as mean ± standard error (SE). Comparisons between experimental groups were performed using the appropriate statistical tests available within GraphPad Prism (nonlinear regression analysis). Differences were considered statistically significant when the *p*-value was less than 0.005. Statistical analysis was used to evaluate the reproducibility, reliability, and significance of the observed differences in physicochemical properties and biological activities among the tested formulations [68,104].

### 4.12. Assessment of Antibacterial Activity Targeting Gram-Negative Bacteria

Gram-negative bacteria *E. coli* (strain SL06/16-1 16S ribosomal RNA gene with accession number KX279366) was a gift obtained from the Department of Biology, College of Science, Kuwait University. Antibacterial activity of the synthesized metal phthalocyanines and their particle formulations was evaluated against *Escherichia coli* using agar well diffusion assays in accordance with Clinical and Laboratory Standards Institute (CLSI) guidelines adopted by Kuwait University [60,105–107]. All microbiological procedures were performed under strict aseptic conditions in a laminar flow cabinet or near a Bunsen burner flame to minimize contamination. Nutrient agar (NA, Sigma Aldrich) plates were prepared according to Difco manufacturer instructions and allowed to stabilize for 48 h before use. Bacterial inocula were prepared by transferring freshly cultured colonies into nutrient broth and adjusting the suspension to approximately $5 \times 10^5$ CFU $mL^{-1}$.

For antibacterial testing, bacterial suspension was uniformly spread onto the surface of sterile nutrient agar plates using a sterile cotton swab to obtain a confluent bacterial lawn. In parallel, agar well diffusion assays were performed by creating uniform wells in the agar using a sterile cork borer, followed by the addition of 100 µL of each metal phthalocyanine formulation into the respective wells. The plates were incubated at 37 °C for 24 h, after which antibacterial activity was assessed by measuring the diameter of the inhibition zones surrounding the disks or wells. The minimum inhibitory zones were determined by measuring the visible growth inhibition using the ruler.

To investigate concentration-dependent antibacterial effects, the metal phthalocyanines and their encapsulated formulations were tested at different concentrations. The diameters of both clear and total inhibition zones were measured using a calibrated ruler and recorded in millimeters (mm). All experiments were performed in triplicate, and the results were expressed as mean values. The observed inhibition zones were used as indicators of antibacterial efficacy, with larger zones corresponding to greater antimicrobial activity against the Gram-negative bacterial strain [105–107].

## 5. Conclusions

In conclusion, the synthesized metal phthalocyanines were successfully designed, synthesized, and thoroughly characterized. Elemental analysis by EDX confirmed the accurate composition of the synthesized agents, while SEM revealed rough and porous surface morphologies. DLS measurements verified the successful loading of the agents. Biological evaluation against HepG2 and MDA-MB-453 cancer cell lines demonstrated significant anticancer activity, particularly for gallium II phthalocyanine, which exhibited the lowest $IC_{50}$ values and the highest overall potency. The encapsulated formulations also showed concentration-dependent antibacterial activity against *Escherichia coli*. The

enhanced biological performance of gallium II phthalocyanine may be attributed to its favorable physicochemical properties and porous nanoscale structure, which can facilitate improved interactions with cellular and bacterial targets. Overall, these findings highlight gallium II phthalocyanine as a promising non-photoactivated candidate for future anticancer and antibacterial applications.

**Supplementary Materials:** The following supporting information can be downloaded at: https://www.mdpi.com/article/10.3390/ijms27167322/s1.

**Author Contributions:** M.A.: Methodology. L.J.-A.: Writing—original draft, writing reviewing and editing, conceptualization, funding, resources. R.A.: Supervision, review and editing, resources. All authors have read and agreed to the published version of the manuscript.

**Funding:** This project was supported and funded by grant number (SC04/25) from Research Sector at Kuwait university.

**Institutional Review Board Statement:** Not applicable.

**Informed Consent Statement:** Not applicable.

**Data Availability Statement:** Data available within the article or its Supplementary Materials.

**Acknowledgments:** The authors appreciate the Research Sector Project Unit (RSPU) at Kuwait University for providing access to research facilities, particularly instruments GS01/03, GS01/05, GS02/01, and GS03/08. In addition, we thank the Nanoscopy Center for the EDX and SEM results for our samples. The authors gratefully acknowledge Fatima Hussain for generously providing the chitosan used in this study. We also extend our sincere gratitude to Saad Makhseed for his valuable guidance in the synthesis.

**Conflicts of Interest:** The authors declare no conflicts of interest.

## References

1. Zhang, Y.; Wu, C.; Zhang, N.; Fan, R.; Ye, Y.; Xu, J. Recent Advances in the Development of Pyrazole Derivatives as Anticancer Agents. *Int. J. Mol. Sci.* **2023**, *24*, 12724. [CrossRef] [PubMed]
2. Yusuf, K.; Sampath, V.; Umar, S. Bacterial Infections and Cancer: Exploring This Association and Its Implications for Cancer Patients. *Int. J. Mol. Sci.* **2023**, *24*, 3110. [CrossRef] [PubMed]
3. Jaragh-Alhadad, L.A. Nano LDL Drug Delivery Systems of Triazole Derivatives: Synthesis, Characterization, Anticancer Evaluation and In silico Investigation Targeting HER2 and β-Tubulin Proteins. *Andrology* **2025**, *14*, 351.
4. Chornovolenko, K.; Koczorowski, T. Phthalocyanines Conjugated with Small Biologically Active Compounds for the Advanced Photodynamic Therapy: A Review. *Molecules* **2025**, *30*, 3297. [CrossRef] [PubMed]
5. Sztanke, M.; Wilk, A.; Sztanke, K. An Insight into Fluorinated Imines and Hydrazones as Antibacterial Agents. *Int. J. Mol. Sci.* **2024**, *25*, 3341. [CrossRef] [PubMed]
6. Tafere, D.A.; Gebrezgiabher, M.; Elemo, F.; Sani, T.; Atisme, T.B.; Ashebr, T.G.; Ahmed, I.N. Hydrazones, hydrazones-based coinage metal complexes, and their biological applications. *RSC Adv.* **2025**, *15*, 6191–6207. [CrossRef] [PubMed]
7. Arshad, M.F.; Alam, A.; Alshammari, A.A.; Alhazza, M.B.; Alzimam, I.M.; Alam, M.A.; Mustafa, G.; Ansari, M.S.; Alotaibi, A.M.; Alotaibi, A.A.; et al. Thiazole: A Versatile Standalone Moiety Contributing to the Development of Various Drugs and Biologically Active Agents. *Molecules* **2022**, *27*, 3994. [CrossRef] [PubMed]
8. Guo, J.; Xie, Z.; Ruan, W.; Tang, Q.; Qiao, D.; Zhu, W. Thiazole-based analogues as potential antibacterial agents against methicillin-resistant Staphylococcus aureus (MRSA) and their SAR elucidation. *Eur. J. Med. Chem.* **2023**, *259*, 115689. [CrossRef] [PubMed]
9. Jaragh-Alhadad, L.; Behbehani, H.; Karnik, S. Cancer targeted drug delivery using active low-density lipoprotein nanoparticles encapsulated pyrimidines heterocyclic anticancer agents as microtubule inhibitors. *Drug Deliv.* **2022**, *29*, 2759–2772. [CrossRef] [PubMed]
10. Venugopala, K.N.; Kamat, V. Pyrimidines: A New Versatile Molecule in the Drug Development Field, Scope, and Future Aspects. *Pharmaceuticals* **2024**, *17*, 1258. [CrossRef] [PubMed]
11. Kong, Q.; Yang, Y. Recent advances in antibacterial agents. *Bioorg. Med. Chem. Lett.* **2021**, *35*, 127799. [CrossRef] [PubMed]
12. Parham, S.; Kharazi, A.Z.; Bakhsheshi-Rad, H.R.; Nur, H.; Ismail, A.F.; Sharif, S.; RamaKrishna, S.; Berto, F. Antioxidant, Antimicrobial and Antiviral Properties of Herbal Materials. *Antioxidants* **2020**, *9*, 1309. [CrossRef] [PubMed]

13. Ullah, A.; Munir, S.; Badshah, S.L.; Khan, N.; Ghani, L.; Poulson, B.G.; Emwas, A.H.; Jaremko, M. Important Flavonoids and Their Role as a Therapeutic Agent. *Molecules* **2020**, *25*, 5243. [CrossRef] [PubMed]
14. Sharifi-Rad, J.; Cruz-Martins, N.; López-Jornet, P.; Lopez, E.P.; Harun, N.; Yeskaliyeva, B.; Beyatli, A.; Sytar, O.; Shaheen, S.; Sharopov, F.; et al. Natural Coumarins: Exploring the Pharmacological Complexity and Underlying Molecular Mechanisms. *Oxid. Med. Cell. Longev.* **2021**, *2021*, 6492346. [CrossRef] [PubMed]
15. Liu, Y.; Liang, Y.; Yuhong, J.; Xin, P.; Han, J.L.; Du, Y.; Yu, X.; Zhu, R.; Zhang, M.; Chen, W.; et al. Advances in Nanotechnology for Enhancing the Solubility and Bioavailability of Poorly Soluble Drugs. *Drug Des. Dev. Ther.* **2024**, *18*, 1469–1495. [CrossRef] [PubMed]
16. Liu, Y.L.; Zhang, Q.; Li, B.Q.; Zhang, D.; Chui, R.H.; Zhang, L.L.; Zhang, Q.; Ma, L.Y. Progress in the study of anti-Alzheimer's disease activity of pyrimidine-containing bioactive molecules. *Eur. J. Med. Chem.* **2025**, *285*, 117199. [CrossRef] [PubMed]
17. Sakamoto, K.; Ohno-Okumura, E. Syntheses and Functional Properties of Phthalocyanines. *Materials* **2009**, *2*, 1127–1179. [CrossRef]
18. Szwajca, A.; Pankiewicz, R. Quantum Chemical Stability Analysis of Phthalocyanine Metal One-Dimensional Polymers with Bidentate Ligands. *Molecules* **2024**, *29*, 4111. [CrossRef] [PubMed]
19. Kavetsou, E.; Tsoukalas-Koulas, C.; Katopodi, A.; Kalospyros, A.; Alexandratou, E.; Detsi, A. Inclusion Complexes of Magnesium Phthalocyanine with Cyclodextrins as Potential Photosensitizing Agents. *Bioengineering* **2023**, *10*, 244. [CrossRef] [PubMed]
20. Ma, S.; Shi, S.; Hu, X.; Zhao, Y.; Yang, B.; Liao, M.; Lu, B.; Xu, Q. From basic to clinical translation: Advances and perspectives of photodynamic nanodrugs. *Front. Pharmacol.* **2025**, *16*, 1606372. [CrossRef] [PubMed]
21. Liu, H.; Li, Z.; Zhang, X.; Xu, Y.; Tang, G.; Wang, Z.; Zhao, Y.Y.; Ke, M.R.; Zheng, B.Y.; Huang, S.; et al. Phthalocyanine aggregates as semiconductor-like photocatalysts for hypoxic-tumor photodynamic immunotherapy. *Nat. Commun.* **2025**, *16*, 326. [CrossRef] [PubMed]
22. Galstyan, A. Turning Photons into Drugs: Phthalocyanine-Based Photosensitizers as Efficient Photoantimicrobials. *Chemistry* **2021**, *27*, 1903–1920. [CrossRef] [PubMed]
23. Sai, D.L.; Lee, J.; Nguyen, D.L.; Kim, Y.P. Tailoring photosensitive ROS for advanced photodynamic therapy. *Exp. Mol. Med.* **2021**, *53*, 495–504. [CrossRef] [PubMed]
24. Jaragh-Alhadad, L.A.; Falahati, M. Copper oxide nanoparticles promote amyloid-β-triggered neurotoxicity through formation of oligomeric species as a prelude to Alzheimer's diseases. *Int. J. Biol. Macromol.* **2022**, *207*, 121–129. [CrossRef] [PubMed]
25. Naeem, N.; Sadiq, A.; Ogaly, H.A.; Mughal, E.U. Phthalocyanine-nanoparticle conjugates for enhanced cancer photodynamic therapy. *RSC Adv.* **2025**, *15*, 29890–29924. [CrossRef] [PubMed]
26. Jaragh-Alhadad, L.A.; Falahati, M. Tin oxide nanoparticles trigger the formation of amyloid β oligomers/protofibrils and underlying neurotoxicity as a marker of Alzheimer's disease. *Int. J. Biol. Macromol.* **2022**, *204*, 154–160. [CrossRef] [PubMed]
27. Jaragh-Alhadad, L.A.; Falahati, M. Tin oxide nanoparticles trigger the formation of amyloid β oligomers/protofibrils and underlying neurotoxicity as a marker of Alzheimer's diseases. *Int. J. Biol. Macromol.* **2022**, *204*, 154–160. [CrossRef] [PubMed]
28. Klojdová, I.; Milota, T.; Smetanová, J.; Stathopoulos, C. Encapsulation: A Strategy to Deliver Therapeutics and Bioactive Compounds? *Pharmaceuticals* **2023**, *16*, 362. [CrossRef] [PubMed]
29. Bhattacharjee, S. Craft of Co-encapsulation in Nanomedicine: A Struggle to Achieve Synergy through Reciprocity. *ACS Pharmacol. Transl. Sci.* **2022**, *5*, 278–298. [CrossRef] [PubMed]
30. Arumugam, M.; Zhang, Y.; Huang, Y.; Perumal, R.K.; Zhang, T.; Kong, X.; Zhao, R. Cell encapsulated biomaterials for translational medicine. *Bioact. Mater.* **2025**, *56*, 402–454. [CrossRef] [PubMed]
31. Rezagholizade-Shirvan, A.; Soltani, M.; Shokri, S.; Radfar, R.; Arab, M.; Shamloo, E. Bioactive compound encapsulation: Characteristics, applications in food systems, and implications for human health. *Food Chem. X* **2024**, *24*, 101953. [CrossRef] [PubMed]
32. Xu, Y.; Yan, X.; Zheng, H.; Li, J.; Wu, X.; Xu, J.; Zhen, Z.; Du, C. The application of encapsulation technology in the food Industry: Classifications, recent Advances, and perspectives. *Food Chem. X* **2024**, *21*, 101240. [CrossRef] [PubMed]
33. Grgić, J.; Šelo, G.; Planinić, M.; Tišma, M.; Bucić-Kojić, A. Role of the Encapsulation in Bioavailability of Phenolic Compounds. *Antioxidants* **2020**, *9*, 923. [CrossRef] [PubMed]
34. He, B.; Yang, Q. Recent Development of LDL-Based Nanoparticles for Cancer Therapy. *Pharmaceuticals* **2022**, *16*, 18. [CrossRef] [PubMed]
35. Padín-González, E.; Lancaster, P.; Bottini, M.; Gasco, P.; Tran, L.; Fadeel, B.; Wilkins, T.; Monopoli, M.P. Understanding the Role and Impact of Poly (Ethylene Glycol) (PEG) on Nanoparticle Formulation: Implications for COVID-19 Vaccines. *Front. Bioeng. Biotechnol.* **2022**, *10*, 882363. [CrossRef] [PubMed]
36. Santhanakrishnan, K.R.; Koilpillai, J.; Narayanasamy, D. PEGylation in Pharmaceutical Development: Current Status and Emerging Trends in Macromolecular and Immunotherapeutic Drugs. *Cureus* **2024**, *16*, e66669. [CrossRef] [PubMed]
37. Jafernik, K.; Ładniak, A.; Blicharska, E.; Czarnek, K.; Ekiert, H.; Wiącek, A.E.; Szopa, A. Chitosan-Based Nanoparticles as Effective Drug Delivery Systems—A review. *Molecules* **2023**, *28*, 1963. [CrossRef] [PubMed]

38. Priya, S.; Desai, V.M.; Singhvi, G. Surface Modification of Lipid-Based Nanocarriers: A Potential Approach to Enhance Targeted Drug Delivery. *ACS Omega* **2022**, *8*, 74–86. [CrossRef] [PubMed]
39. Herdiana, Y.; Levita, J.; Jiranusornkul, S. Chitosan-Based Nanoparticles Targeted Delivery System: In Treatment Approach for Dyslipidemia. *Int. J. Nanomed.* **2025**, *20*, 6611–6636. [CrossRef] [PubMed]
40. Abdellatif, A.A.H. A plausible way for excretion of metal nanoparticles *via* active targeting. *Drug Dev. Ind. Pharm.* **2020**, *46*, 744–750. [CrossRef] [PubMed]
41. Abdellatif, A.A.H.; Alturki, H.; Tawfeek, H.M. Different cellulosic polymers for synthesizing silver nanoparticles with antioxidant and antibacterial activities. *Sci. Rep.* **2021**, *11*, 84. [CrossRef] [PubMed]
42. Fahmy, S.A.; Ramzy, A.; Mandour, A.A.; Nasr, S.; Abdelnaser, A.; Bakowsky, U.; Azzazy, H.M.E. PEGylated Chitosan Nanoparticles Encapsulating Ascorbic Acid and Oxaliplatin Exhibit Dramatic Apoptotic Effects against Breast Cancer Cells. *Pharmaceutics* **2022**, *14*, 407, Correction in *Pharmaceutics* **2026**, *18*, 511. https://doi.org/10.3390/pharmaceutics18040511. [CrossRef] [PubMed]
43. Jin, X.; Guo, F.; Wu, M.; Xu, C.; Li, Y.; Chen, G. Emerging versatile nanozymes for the therapeutic and diagnostic applications of diseases. *J. Transl. Med.* **2025**, *23*, 1375. [CrossRef] [PubMed]
44. Chakraborty, N.; Gandhi, S.; Verma, R.; Roy, I. Emerging Prospects of Nanozymes for Antibacterial and Anticancer Applications. *Biomedicines* **2022**, *10*, 1378. [CrossRef] [PubMed]
45. Nan, F.; Jia, Q.; Xue, X.; Wang, S.; Liu, W.; Wang, J.; Ge, J.; Wang, P. Iron phthalocyanine-derived nanozyme as dual reactive oxygen species generation accelerator for photothermally enhanced tumor catalytic therapy. *Biomaterials* **2022**, *284*, 121495. [CrossRef] [PubMed]
46. Nackiewicz, J.; Kliber-Jasik, M.; Pogoda-Mieszczak, K.; Skonieczna, M. Gallium octacarboxyphthalocyanine hydroxide as a potential pro-apoptotic drug against cancer skin cells. *Bioorg. Chem.* **2024**, *152*, 107736. [CrossRef] [PubMed]
47. Papadopoulos, Z.; Antar, Y.; Dieter, I.S.; Peeters, F.; Plaza-Sirvent, C.; Karges, J. Gallium(III) Complex Induces Immunogenic Cell Death Hallmarks for Chemoimmunotherapy. *J. Med. Chem.* **2025**, *68*, 15980–15990. [CrossRef] [PubMed]
48. Sánchez-López, E.; Gomes, D.; Esteruelas, G.; Bonilla, L.; Lopez-Machado, A.L.; Galindo, R.; Cano, A.; Espina, M.; Ettcheto, M.; Camins, A.; et al. Metal-Based Nanoparticles as Antimicrobial Agents: An Overview. *Nanomaterials* **2020**, *10*, 292. [CrossRef] [PubMed]
49. Mammari, N.; Lamouroux, E.; Boudier, A.; Duval, R.E. Current Knowledge on the Oxidative-Stress-Mediated Antimicrobial Properties of Metal-Based Nanoparticles. *Microorganisms* **2022**, *10*, 437. [CrossRef] [PubMed]
50. Bonelli, J.; Ortega-Forte, E.; Vigueras, G.; Follana-Berná, J.; Ashoo, P.; Abad-Montero, D.; Isidro, N.; López-Corrales, M.; Hernández, A.; Ortiz, J.; et al. A Nanoencapsulated Ir(III)-Phthalocyanine Conjugate as a Promising Photodynamic Therapy Anticancer Agent. *ACS Appl. Mater. Interfaces* **2024**, *16*, 38916–38930. [CrossRef] [PubMed]
51. Ying, J.F.; Lu, Z.B.; Fu, L.Q.; Tong, Y.; Wang, Z.; Li, W.F.; Mou, X.Z. The role of iron homeostasis and iron-mediated ROS in cancer. *Am. J. Cancer Res.* **2021**, *11*, 1895–1912. [PubMed]
52. Alfei, S.; Schito, G.C.; Schito, A.M.; Zuccari, G. Reactive Oxygen Species (ROS)-Mediated Antibacterial Oxidative Therapies: Available Methods to Generate ROS and a Novel Option Proposal. *Int. J. Mol. Sci.* **2024**, *25*, 7182. [CrossRef] [PubMed]
53. Mohamed, H.R.H.; Mohamed, B.A.; Hakeem, G.M.; Elnawasani, S.H.; Nagy, M.; Essam, R.; Diab, A.; Safwat, G. Cobalt oxide nanoparticles induce cytotoxicity and excessive ROS mediated mitochondrial dysfunction and p53-independent apoptosis in melanoma cells. *Sci. Rep.* **2025**, *15*, 2220. [CrossRef] [PubMed]
54. Morari, V.; Lungu, I.; Suman, V.; Ghimpu, L.; Potlog, T.; Tigoianu, R.; Stoica, I.; Gherasim, C.; Airinei, A. Spectral Relationships of ZnPc and CuPc: UV-VIS and Fluorescence Behavior in Liquids and Thin Films. *Molecules* **2025**, *30*, 4262. [CrossRef] [PubMed]
55. Escayola, S.; Labella, J.; Szczepanik, D.W.; Poater, A.; Torres, T.; Solà, M.; Matito, E. From (Sub)Porphyrins to (Sub)Phthalocyanines: Aromaticity Signatures in the UV-Vis Absorption Spectra. *Inorg. Chem.* **2024**, *63*, 18251–18262. [CrossRef] [PubMed]
56. Sánchez Vergara, M.E.; Vargas, M.G.; Sandoval Plata, E.I.; Huerta, A.F. Chloro-substituted metallo-phthalocyanines (TiPcCl2, MnPcCl, InPcCl, AlPcCl) applied to organic devices. *Heliyon* **2025**, *11*, e42697. [CrossRef] [PubMed]
57. Kawauchi, K.; Urano, R.; Kinoshita, N.; Kuwamoto, S.; Torii, T.; Hashimoto, Y.; Taniguchi, S.; Tsuruta, M.; Miyoshi, D. Photosensitizers Based on G-Quadruplex Ligand for Cancer Photodynamic Therapy. *Genes* **2020**, *11*, 1340. [CrossRef] [PubMed]
58. Cao, H.; Gong, M.; Wang, M.; Tang, Q.; Wang, L.; Zheng, X. Steady/transient state spectral researches on the solvent-triggered and photo-induced novel properties of metal-coordinated phthalocyanines. *RSC Adv.* **2022**, *12*, 5964–5970. [CrossRef] [PubMed]
59. Ramos, A.A.; Nascimento, F.B.; de Souza, T.F.; Omori, A.T.; Manieri, T.M.; Cerchiaro, G.; Ribeiro, A.O. Photochemical and Photophysical Properties of Phthalocyanines Modified with Optically Active Alcohols. *Molecules* **2015**, *20*, 13575–13590. [CrossRef] [PubMed]
60. Alshehab, A.; Haider, A.; Jaragh-Alhadad, L. Significance of Nano Transition Metal Complexes as Anticancer and Antibacterial Therapeutic Agents. *Int. J. Mol. Sci.* **2025**, *26*, 10516. [CrossRef] [PubMed]
61. Bernal-Chávez, S.A.; Del Prado-Audelo, M.L.; Caballero-Florán, I.H.; Giraldo-Gomez, D.M.; Figueroa-Gonzalez, G.; Reyes-Hernandez, O.D.; González-Del Carmen, M.; González-Torres, M.; Cortés, H.; Leyva-Gómez, G. Insights into Terminal Sterilization Processes of Nanoparticles for Biomedical Applications. *Molecules* **2021**, *26*, 2068. [CrossRef] [PubMed]

62. González-González, O.; Ramirez, I.O.; Ramirez, B.I.; O'Connell, P.; Ballesteros, M.P.; Torrado, J.J.; Serrano, D.R. Drug Stability: ICH versus Accelerated Predictive Stability Studies. *Pharmaceutics* **2022**, *14*, 2324. [CrossRef] [PubMed]
63. Lutzweiler, G.; Ndreu Halili, A.; Engin Vrana, N. The Overview of Porous, Bioactive Scaffolds as Instructive Biomaterials for Tissue Regeneration and Their Clinical Translation. *Pharmaceutics* **2020**, *12*, 602. [CrossRef] [PubMed]
64. Yao, Y.; Zhou, Y.; Liu, L.; Xu, Y.; Chen, Q.; Wang, Y.; Wu, S.; Deng, Y.; Zhang, J.; Shao, A. Nanoparticle-Based Drug Delivery in Cancer Therapy and Its Role in Overcoming Drug Resistance. *Front. Mol. Biosci.* **2020**, *7*, 193. [CrossRef] [PubMed]
65. Li, S.R.; Huo, F.Y.; Wang, H.Q.; Wang, J.; Xu, C.; Liu, B.; Bu, L.L. Recent advances in porous nanomaterials-based drug delivery systems for cancer immunotherapy. *J. Nanobiotechnol.* **2022**, *20*, 277. [CrossRef] [PubMed]
66. Tarighi, P.; Mousavi Esfahani, S.M.; Emamjomeh, A.; Mirjalili, S.Z.; Mirzabeigi, P. Optimizing Cancer Treatment: A Comprehensive Review of Active and Passive Drug Delivery Strategies. *Iran. Biomed. J.* **2025**, *29*, 173–188. [CrossRef] [PubMed]
67. Jaragh-Alhadad, L.A.; Ali, M.S. Nimesulide derivatives reduced cell proliferation against breast and ovarian cancer: Synthesis, characterization, biological assessment, and crystal structure. *Kuwait J. Sci.* **2022**, *49*, 1–17. [CrossRef]
68. Ali, M.S.; Kuraijam, D.; Karnik, S.; Jaragh-Alhadad, L.A. Hydrazone bimetallic complex: Synthesis, characterization, in silico and biological evaluation targeting breast and lung cancer cells' G-quadruplex DNA. *Kuwait J. Sci.* **2023**, *50*, 1–17. [CrossRef]
69. Draviana, H.T.; Fitriannisa, I.; Khafid, M.; Krisnawati, D.I.; Widodo; Lai, C.H.; Fan, Y.J.; Kuo, T.R. Size and charge effects of metal nanoclusters on antibacterial mechanisms. *J. Nanobiotechnol.* **2023**, *21*, 428. [CrossRef] [PubMed]
70. Al-Shadidi, J.R.M.H.; Al-Shammari, S.; Al-Mutairi, D.; Alkhudhair, D.; Thu, H.E.; Hussain, Z. Chitosan Nanoparticles for Targeted Cancer Therapy: A Review of Stimuli-Responsive, Passive, and Active Targeting Strategies. *Int. J. Nanomed.* **2024**, *19*, 8373–8400. [CrossRef] [PubMed]
71. Kim, J.; Lee, S.; Na, K. Glycyrrhetinic Acid-Modified Silicon Phthalocyanine for Liver Cancer-Targeted Photodynamic Therapy. *Biomacromolecules* **2023**, *22*, 811–822. [CrossRef] [PubMed]
72. Deng, C.F.; Zhu, N.; Zhao, T.J.; Li, H.F.; Gu, J.; Liao, D.F.; Qin, L. Involvement of LDL and ox-LDL in Cancer Development and Its Therapeutical Potential. *Front. Oncol.* **2022**, *12*, 803473. [CrossRef] [PubMed]
73. Carobeli, L.R.; Meirelles, L.E.F.; Damke, G.M.Z.F.; Damke, E.; de Souza, M.V.F.; Mari, N.L.; Mashiba, K.H.; Shinobu-Mesquita, C.S.; Souza, R.P.; da Silva, V.R.S.; et al. Phthalocyanine and Its Formulations: A Promising Photosensitizer for Cervical Cancer Phototherapy. *Pharmaceutics* **2021**, *13*, 2057. [CrossRef] [PubMed]
74. Borzęcka, W.; Domiński, A.; Kowalczuk, M. Recent Progress in Phthalocyanine-Polymeric Nanoparticle Delivery Systems for Cancer Photodynamic Therapy. *Nanomaterials* **2021**, *11*, 2426. [CrossRef] [PubMed]
75. Rak, J.; Kabesova, M.; Benes, J.; Pouckova, P.; Vetvicka, D. Advances in Liposome-Encapsulated Phthalocyanines for Photodynamic Therapy. *Life* **2023**, *13*, 305. [CrossRef] [PubMed]
76. Guo, L.; Li, Y.; Feng, J.; Li, Y.; Liao, Y.; Zeng, Q.; Li, Y.; Yang, L.; Li, J.; Liu, C.; et al. Antibacterial activity and potential mechanisms of plumbagin against *Escherichia coli* and its application in milk. *Curr. Res. Food Sci.* **2025**, *10*, 101083. [CrossRef] [PubMed]
77. Kircheva, N.; Dobrev, S.; Petkova, V.; Yocheva, L.; Angelova, S.; Dudev, T. In Silico Analysis of the Ga3+/Fe3+ Competition for Binding the Iron-Scavenging Siderophores of *P. aeruginosa*—Implementation of Three Gallium-Based Complexes in the "Trojan Horse" Antibacterial Strategy. *Biomolecules* **2024**, *14*, 487. [CrossRef] [PubMed]
78. Xie, W.; Xu, Z. (Nano)biotechnological approaches in the treatment of cervical cancer: Integration of engineering and biology. *Front. Immunol.* **2024**, *15*, 1461894. [CrossRef] [PubMed]
79. Menichetti, A.; Mavridi-Printezi, A.; Mordini, D.; Montalti, M. Effect of Size, Shape and Surface Functionalization on the Antibacterial Activity of Silver Nanoparticles. *J. Funct. Biomater.* **2023**, *14*, 244. [CrossRef] [PubMed]
80. Alidriss, O.M.; AlSudais, H.; Alhumaidan, O.S.; Altwaijry, H.D.; Bakhsh, A.; Almuhanna, Y.; Alkudmani, Z.S.; Alqarni, I.A.; Alenazi, D.; Aljasham, A.T.; et al. Targeted Drug Delivery Strategies in Overcoming Antimicrobial Resistance: Advances and Future Directions. *Pharmaceutics* **2025**, *17*, 1426. [CrossRef] [PubMed]
81. Li, B.; Liao, Y.; Su, X.; Chen, S.; Wang, X.; Shen, B.; Song, H.; Yue, P. Powering mesoporous silica nanoparticles into bioactive nanoplatforms for antibacterial therapies: Strategies and challenges. *J. Nanobiotechnol.* **2023**, *21*, 325. [CrossRef] [PubMed]
82. AlQurashi, D.M.; AlQurashi, T.F.; Alam, R.I.; Shaikh, S.; Tarkistani, M.A.M. Advanced Nanoparticles in Combating Antibiotic Resistance: Current Innovations and Future Directions. *J. Nanotheranostics* **2025**, *6*, 9. [CrossRef]
83. Rodriguez-Loya, J.; Lerma, M.; Gardea-Torresdey, J.L. Dynamic Light Scattering and Its Application to Control Nanoparticle Aggregation in Colloidal Systems: A Review. *Micromachines* **2023**, *15*, 24. [CrossRef] [PubMed]
84. Saraswati, L.D.; Widjanarko, B.; Herawati, V.E.; Fauziah, A.I. The Effects of Chitosan-PEG Nanoparticles Based on Channa striata Protein Hydrolyzate on Decreasing Diabetes Mellitus in Diabetic Rats. *Ethiop. J. Health Sci.* **2022**, *32*, 833–840. [CrossRef] [PubMed]
85. Hosseini, M.; Ezzeddini, R.; Hashemi, S.M.; Soudi, S.; Salek Farrokhi, A. Enhanced anti-tumor efficacy of S3I-201 in breast cancer mouse model through Wharton jelly- exosome. *Cancer Cell Int.* **2024**, *24*, 318. [CrossRef] [PubMed]
86. Wang, M.; Wang, Y.; Chen, G.; Gao, H.; Peng, Q. Chitosan-Based Multifunctional Biomaterials as Active Agents or Delivery Systems for Antibacterial Therapy. *Bioengineering* **2024**, *11*, 1278. [CrossRef] [PubMed]

87. Akdaşçi, E.; Duman, H.; Eker, F.; Bechelany, M.; Karav, S. Chitosan and Its Nanoparticles: A Multifaceted Approach to Antibacterial Applications. *Nanomaterials* **2025**, *15*, 126. [CrossRef] [PubMed]
88. Ahmad, N.; Khan, M.R.; Palanisamy, S.; Mohandoss, S. Anticancer Drug-Loaded Chitosan Nanoparticles for In Vitro Release, Promoting Antibacterial and Anticancer Activities. *Polymers* **2023**, *15*, 3925. [CrossRef] [PubMed]
89. Tawfik, A.; Farid, A. Chitosan-encapsulated *Aloe vera* nanoparticles outperform carrier-free forms in enhancing MSCs therapy for amikacin nephrotoxicity. *Sci. Rep.* **2025**, *15*, 34292. [CrossRef] [PubMed]
90. Li, Y.; Li, X.M.; Wei, L.S.; Ye, J.F. Advancements in mitochondrial-targeted nanotherapeutics: Overcoming biological obstacles and optimizing drug delivery. *Front. Immunol.* **2024**, *15*, 1451989. [CrossRef] [PubMed]
91. Buchke, S.; Sharma, M.; Bora, A.; Relekar, M.; Bhanu, P.; Kumar, J. Mitochondria-Targeted, Nanoparticle-Based Drug-Delivery Systems: Therapeutics for Mitochondrial Disorders. *Life* **2022**, *12*, 657. [CrossRef] [PubMed]
92. Di, L.; Maiseyeu, A. Low-density lipoprotein nanomedicines: Mechanisms of targeting, biology, and theranostic potential. *Drug Deliv.* **2021**, *28*, 408–421. [CrossRef] [PubMed]
93. Cahn, D.; Pal, S.; Stern, A.; Patel, N.L.; Gower, T.; Kapnick, S.M.; Jewell, C.M.; Duncan, G.A.; Wolf, M.T. PEGylation strategies for enhanced nanoparticle delivery to tumor-associated immune cells. *Bioeng. Transl. Med.* **2025**, *11*, e70098. [CrossRef] [PubMed]
94. Mahmudi, H.; Adili-Aghdam, M.A.; Shahpouri, M.; Jaymand, M.; Amoozgar, Z.; Jahanban-Esfahlan, R. Tumor microenvironment penetrating chitosan nanoparticles for elimination of cancer relapse and minimal residual disease. *Front. Oncol.* **2022**, *12*, 1054029. [CrossRef] [PubMed]
95. Wysocki, M.; Ziental, D.; Biyiklioglu, Z.; Jozkowiak, M.; Dlugaszewska, J.; Piotrowska-Kempisty, H.; Güzel, E.; Sobotta, L. Axially Disubstituted Silicon(IV) Phthalocyanine as a Potent Sensitizer for Antimicrobial and Anticancer Photo and Sonodynamic Therapy. *Int. J. Mol. Sci.* **2025**, *26*, 7447. [CrossRef] [PubMed]
96. Al-Sawah, M.; Abdel Nazeer, A.; Salah, L.; Durmuş, M.; Makhseed, S. Novel azaphthalocyanines with efficient anti-corrosion capability: Effect of halogens and heavy metals. *J. Mol. Liq.* **2019**, *293*, 111545. [CrossRef]
97. Durmuş, M.; Nyokong, T. Synthesis, photophysical and photochemical properties of tetra- and octa-substituted gallium and indium phthalocyanines. *Polyhedron* **2007**, *26*, 3323–3335. [CrossRef]
98. Thanuj, S. Unlocking the Secrets of Molecules with UV-Vis Spectroscopy. *Pharm. Anal. Chem.* **2023**, *8*, 186.
99. Andure, S.D.; Tiwari, N. A Complete Review on UV-Visible Spectroscopic Technique. *Int. J. Pharm. Res. Appl.* **2022**, *7*, 1288–1299.
100. Aguilar-Toalá, J.E.; Quintanar-Guerrero, D.; Liceaga, A.M.; Zambrano-Zaragoza, M.L. Encapsulation of bioactive peptides: A strategy to improve the stability, protect the nutraceutical bioactivity and support their food applications. *RSC Adv.* **2022**, *12*, 6449–6458. [PubMed]
101. Jia, Z.; Li, J.; Gao, L.; Yang, D.; Kanaev, A. Dynamic Light Scattering: A Powerful Tool for In Situ Nanoparticle Sizing. *Colloids Interfaces* **2023**, *7*, 15. [CrossRef]
102. Sylvester, P.W. Optimization of the tetrazolium dye (MTT) colorimetric assay for cellular growth and viability. *Methods Mol. Biol.* **2011**, *716*, 157–168. [CrossRef] [PubMed]
103. Ali, M.S.; El-Saied, F.A.; Shakdofa, M.M.E.; Karnik, S.; Jaragh-Alhadad, L.A. Synthesis and characterization of thiosemicarbazone metal complexes: Crystal structure, and antiproliferation activity against breast (MCF7) and lung (A549) cancers. *J. Mol. Struct.* **2023**, *1274*, 134485. [CrossRef]
104. Jaragh-Alhadad, L.; Samir, M.; Harford, T.J.; Karnik, S. Low-density lipoprotein encapsulated thiosemicarbazone metal complexes is active targeting vehicle for breast, lung, and prostate cancers. *Drug Deliv.* **2022**, *29*, 2206–2216. [CrossRef] [PubMed]
105. Sribenjalux, W.; Kulwongroj, P.; Kuwatjanakul, W.; Wonglakorn, L.; Srisak, K.; Manomaiwong, N.; Meesing, A. Direct Disk Diffusion Testing and Antimicrobial Stewardship for Gram-Negative Bacteremia in the Context of High Multidrug Resistance. *Antibiotics* **2025**, *14*, 726. [CrossRef] [PubMed]
106. AL-Hussein, W.K.; Jaragh-Alhadad, L.A. In vitro experimental and computational study of 1,2,4-triazole derivatives as antimicrobial and anticancer agents. *Kuwait J. Sci.* **2026**, *53*, 100557. [CrossRef]
107. Ali, A.; Zhang, N.; Santos, R.M. Mineral Characterization Using Scanning Electron Microscopy (SEM): A Review of the Fundamentals, Advancements, and Research Directions. *Appl. Sci.* **2023**, *13*, 12600. [CrossRef]


**Disclaimer/Publisher's Note:** The statements, opinions and data contained in all publications are solely those of the individual author(s) and contributor(s) and not of MDPI and/or the editor(s). MDPI and/or the editor(s) disclaim responsibility for any injury to people or property resulting from any ideas, methods, instructions or products referred to in the content.